Title:

CREB-binding protein gene, *HAC701*, negatively regulates WRKY45-dependent immunity in rice

Running title:

HAC701-dependent immunity regulation

Authors:

Nino A. Espinas[1,3,*], Tu Ngoc Le[1], Saori, Miura[1], Yasuka Shimajiri[1,2], Ken Shirasu[3], Hidetoshi Saze[1]

Affiliation:

[1]Plant Epigenetics Unit, Okinawa Institute of Science and Technology Graduate University, Onna-son, Okinawa, Japan

[2]EditForce, Fukuoka, Japan

[3]RIKEN Center for Sustainable Resource Science, Yokohama, Kanagawa, Japan

Contact:

[*]Correspondence to: Nino A. Espinas (nino.espinas@riken.jp)

Category:

Biological Sciences, Plant Biology

SIGNIFICANCE

HAC701 is a member of CREB-binding protein (CBP) family that acts as transcriptional coactivator and acetyltransferase. However, little is known how it regulates innate immunity in plants. Herein we reported that rice *HAC701* suppresses WRKY45-dependent defense pathway. Our study showed that *HAC70* seemingly interacts genetically with *WRKY45* in rice to modulate immune responses against pathogens.

ABSTRACT

CREB-binding protein (CBP) is a known transcriptional coactivator and an acetyltransferase that functions in several cellular processes by regulating gene expression. However, how it functions in plant immunity remains unexplored. By characterizing *hac701*, we demonstrate that *HAC701* negatively regulates the immune responses in rice. *hac701* show enhanced disease resistance against a bacterial pathogen, *Pseudomonas syringae* pv. *oryzae* (*Pso*), which causes bacterial halo blight of rice. Our transcriptomic analysis revealed that rice *WRKY45*, one of the main regulators of rice immunity, is upregulated in *hac701* and possibly conferring the resistance phenotype against *Pso*. The morphological phenotypes of *hac701* single mutants were highly similar to *WRKY45* overexpression transgenic lines reported in previous studies. In addition, differentially expressed genes (DEGs) in *hac701* largely overlap with genes when *WRKY45* is overexpressed and chemically induced transiently. When we investigated for *cis*-elements found 1kb upstream of *WRKY45* gene and WRKY45-dependent DEGs, we found that *WRKY45* promoter contains the CRE motif, a possible target of HAC701-mediated regulation. Genome-wide H3K9 acetylation profiling showed depletion of acetylation at large set of genes in *hac701*. However, consistent with the upregulation of *WRKY45* gene expression, our ChIP-sequencing analysis demonstrated that regions of *WRKY45* promoter are enriched in H3K9 acetylation in *hac701* compared to the segregated wild type control. Finally, we show that *HAC701* may have roles in systemic immune signaling. We therefore propose that wild type *HAC701* negatively regulates *WRKY45* gene expression, thereby suppressing immune responses.

Keywords:

Oryza sativa, rice CREB-binding protein, *HAC701*, *WRKY45*, innate immunity, *Pseudomonas syringae* pv. *oryzae* (*Pso*), *Magnaporthe*

INTRODUCTION

Histone acetyltransferases (HATs) are a diverse group of histone- and non-histone-modifying enzymes that contain multiple subunits to enable catalytic functions (1). These HATs primarily function as scaffolding bridges of proteins to form the transcriptional regulatory complex important for target recognition and subsequent substrate modification (1-3). The association of HATs to its interacting proteins and the existing state of the epigenome dictates the dual-switch functionality of either transcriptional activation or repression (1). They are considered integrators or adaptors as they were shown to interact with DNA-binding activators and the basal transcriptional machinery (4, 5).

In plant model Arabidopsis, HATs and histone deacetylases (HDACs) are grouped into four (Figure 1A) and three families, respectively (6). HATs consists of CBP, TAF1/TAFII250, GNAT, and MYST, while HDACs are RPD3/HDA1, HD2-like, and SIR2. A previous review of HATs and HDACs in plants listed about 12 putative HAT and 18 HDAC proteins exhibiting acetylation and deacetylation activities with differential site specificities (6). Work on rice (*Oryza sativa*), however, has just begun with a preliminary investigation of eight histone acetyltransferases (7, 8) and deacetylases (9).

Several studies have shown that histone acetylation and deacetylation control defense signaling in plants in response to phytohormone or pathogen application (10-12). More specifically, HATs and HDACs in rice model were shown to be responsive to abiotic stresses and can be modulated by phytohormones, thus implicating a role in biotic stresses (7, 13). Similar to Arabidopsis, HATs in rice are also classified into four families (Figure 1A) (7). In contrary, rice HDACs are represented in only two families, RPD3/HDA1-like and SIR2-like with no known rice member belonging to HD2 family (9).

OsHAC701 was reported (14) earlier as a putative rice CBP-related acetyltransferase, herein after referred to as *HAC701*, of the p300/CBP acetyltransferase (PCAT) family of proteins. The Arabidopsis genome contains five CBP genes, while rice genome contains three (Figure 1A), having broad acetyltransferase specificity on histones (7). Currently, there is no clear consensus on the similarity of biological functions of Arabidopsis and rice homologs of CBP family proteins. In animals, p300 and CBP are paralogs and originally described as transcriptional coactivator that exhibit histone acetyltransferase activity on all four core histones specifically at H4 N-terminal tail sites K5, K8, K12, and K16 (15, 16). Other sites include H3 sites K14, 23 (17), K18, K27 (18, 19), and K56 (20); H2B sites are K12 and K15 (21). H3K9 is mainly acetylated by GCN5/PCAF (18), however acetylation by p300/CBP was also reported (17, 22, 23). Its highly conserved function is mainly found in multicellular organisms as it probably participates in complex physiological processes acting as a limiting factor in various pathways due to its high cellular demand (14).

As HATs have been shown to be modulated by biotic stresses (24), we hypothesized that it could be a potential system for studying rice immunity. Indeed, we show that *HAC701* is involved in rice innate immunity. In this study, we have made CRISPR/Cas9 edited *hac701* and showed that *HAC701* is apparently a negative regulator of immunity with the mutants showing resistance against bacterial and fungal infection. Further transcriptomic investigation showed that HAC701 possibly regulates *WRKY45* loci, one of the main regulators of rice immunity pathways. In *hac701*, *WRKY45* and its direct and indirect gene targets were upregulated upon pathogen inoculation. In addition, *hac701* phenocopies *WRKY45*-overexpression (*WRKY45-ox*) lines, indicating a potential interaction between *HAC701* and *WRKY45*-dependent immunity pathway in rice.

RESULTS

Characterization of a rice acetyltransferase mutant, *HAC701*.

We isolated null mutant lines by independently targeting two sites of *HAC701* gene (Fig. S1A-C; Fig. S1D-I) using CRISPR/Cas9 editing technology. From the 11 positive *HAC701* lines, we have isolated four biallelic homozygous mutant lines (Target2; Fig. S1D), which we utilized for experimentation including their segregating wild type siblings, 9-WT (Fig. 1B). The phenotype in terms of effective grain number and tiller number of mostly all biallelic homozygous mutants at T2 generation did not show impairment as compared to 9-WT (Fig. S1F). In addition, the T3 lines did not show any visible growth or developmental defect in height and photosynthesis (*e.g.* chlorosis phenotype) (Fig. S1G), respectively. However, the weights of 1000-grain T3 and T4 generations of mutants were increased compared to 9-WT (Fig. S1I). These results indicate that a loss of HAC701 does not cause severe developmental defects in rice, and that HAC701 may have a positive role in seed production.

HAC701 mutant rice is resistant to pathogen infection.

Our expression analysis of the rice HAT genes showed that HAC701 is significantly up-regulated by treatment of bacterial flg22 peptide, suggesting a potential role of HAC701 in plant defense against pathogens (Fig. S2). To investigate involvement of *HAC701* in basal defense in rice, we inoculated 9-WT and *HAC701* mutant lines, *9-12b*$^{-/-}$ and *9-5*$^{-/-}$ (hereafter collectively termed *hac701* unless otherwise specified) with mock (10 mM $MgCl_2$) and *Pseudomonas syringae* pv. *oryzae* (*Pso*) (OD = 0.2; resuspended in 10 mM $MgCl_2$) for 72 h (Fig. 1D). *Pso* is a causative agent of halo blight in rice characterized by brown lesions and yellow halo-like blotches on leaves (25). Infection of *Pso* showed that *hac701* (*9-12a*$^{-/-}$, *9-12b*$^{-/-}$ and *9-5*$^{-/-}$) were resistant to *Pso*-treatment as compared to 9-WT (Fig. 1C, S3). These data suggest that *HAC701* might be involved in the regulation of rice innate immunity acting

in its capacity as a transcriptional coactivator and/or as an acetyltransferase. We further tested whether *hac701* also show resistance phenotype when infected with a rice blast pathogen, *Magnaporthe oryzae*. Although the data were not statistically significant, results showed a resistant phenotype tendency in *hac701* (Fig. 1D). Overall, these indicate that *HAC701* plays a negative role in rice innatee immunity.

Transcriptome profiling of the rice-*Pso* pathosystem.

To profile the genome-wide effect of *HAC701* mutation in rice innate immunity, we performed RNA-sequencing on mock- and *Pso*-treated 9-WT and *hac701* using local leaf tissues (Fig. S4; Table S2). We first characterized the effect of *Pso* infection on 9-WT and analysis of the highly variable genes in mock- and *Pso*-treated 9-WT plants showed gene clusters that were dependent on *Pso* induction alone (Fig. S4; Fig. S5). The top 10 highly variable genes across the 9-WT samples showed features involved in tolerance and/or resistance such as disease resistance and stress tolerance mostly by catalysis of primary and secondary metabolism (Fig. S5). This includes well-documented genes involved in plant resistance against pathogens, such as tryptophan decarboxylase 1 (Os08g0140300) that catalyzes the production of serotonin via conversion of tryptophan to tryptamine in rice (26), which has been implicated to confer resistance in rice infected with *Bipolaris oryzae* (27). Another gene, naringenin 7-O-methyltransferase (Os12g0240900), that catalyzes the production of rice phytoalexin sakuranetin has been reported to participate in rice defenses via JA signaling (28, 29). Lignin and phytoalexin encoding genes for instance laccases (*e.g.* Os12g0258700, Os11g0641500) and cytochrome P450s (*e.g.* Os07g0218700, Os08g0508000) are metabolic products known to be involved in plant defenses as well (30-32). Gene Ontology (GO) analysis of upregulated genes in *Pso*-infected 9-WT plants revealed enrichment of genes involved in response to biotic stimulus (GO terms: Response to wounding, Response to other organism, Cell wall macromolecule catabolic process, *etc.*)

(Fig. S6). Both up and downregulated genes showed enrichment of transcriptional machinery regulation, a possible consequence of defense-related transcriptional reprogramming processes during bacterial invasion. GO analysis also identified pathways associated with upregulated gene networks involved in plant defense such as diterpene phytoalexin biosynthetic pathway and chorismate biosynthesis. Thus, the rice-*Pso* pathosystem is a functional system that can be utilized to analyze defense responses of *Pso*-infected rice as well as *Pso* pathogenicity.

Potentiated WRKY45 gene in *hac701* provides resistance against *Pseudomonas* and *Magnaporthe* infections. To investigate the molecular basis of resistance phenotype observed in *Pso*-infected *hac701*, we further analyzed our transcriptome data and found 141 upregulated genes in *hac701* (Fig. S7A; Table S3). We refer to these genes as *HAC701*-repressed genes. GO analysis of *HAC701*-repressed genes showed enrichment of processes involved in response to xenobiotic stimuli and defense response (GO terms: Response to xenobiotic stimulus, Response to wounding, Regulation of defense response, Jasmonic acid mediated signaling pathway, Defense response, *etc.*). These genes were normally not upregulated in the 9-WT background. On the other hand, 336 upregulated genes in the 9-WT background alone referred to as *HAC701*-dependent genes did not show a very distinct enrichment of genes in defense responses rather showed a more general biological and physiological processes (GO terms: Mitochondrial respiratory chain complex IV assembly, Alanine transport, Cellular response to heat, *etc.*) (Fig. S7A; Table S4). We also looked into the features of 31 downregulated genes in the mutant background referred to as *HAC701*-enhanced genes (Fig. S7B; Table S3). These genes were not normally downregulated in the 9-WT background. *HAC701*-enhanced genes contained genes enriched in photosynthetic and response to abiotic stress terms (GO terms: Glycerolipid biosynthetic pathway, Response to cold, Photosynthesis, *etc.*). In addition, the remaining 46 downregulated genes in the 9-WT

background alone also showed a more general biological processes with no hint of enrichment in defense response against pathogen infection (GO terms: Chloroplast organization, Gluconeogenesis, Organelle fission, *etc.*) (Fig. S7B; Table S4).

We were intrigued what genes can be upregulated in *HAC701* mutant background without *Pso*-treatment. Thus, we overlapped the list of genes derived from mock and *Pso*-treated mutants, and found *WRKY45* (*OsWRKY45*) upregulated in the *hac701* background (Fig. 2A; Table S5, S6). *WRKY45* was also identified as one of the 141 upregulated genes in *Pso*-infected *HAC701* mutant (Fig. S7A). There was no candidate gene found downregulated in *HAC701* mutant background alone (Fig. 2A). We then checked whether there were differences in the upregulation strength of *WRKY45* in the *HAC701* mutation alone, compared to *HAC701* mutation combined with *Pso*-treatment. Transcriptome data revealed that *WRKY45* expression was increased by about 20% change upon *Pso*-treatment (Fig. 2B). These results suggest that upregulation of *WRKY45* expression is partially dependent on HAC701 expression. Additional *Pso*-treatment further upregulated *WRKY45* and this subtle increase in expression allowed the co-expression of possibly direct and indirect genes regulated by *WRKY45*.

***hac701* phenocopy *WRKY45* overexpression transgenic plants.**

To determine whether the upregulation of *WRKY45* in *hac701* is relevant to rice with overexpressed *WRKY45* gene, we compared the differentially expressed genes (DEGs) in our *hac701* with *WRKY45* overexpression (*WRKY45-ox*) lines previously reported (in these studies: 33, 34). Our results indicated a striking similarity for targeted genes from rice samples despite the fact that they were inoculated with two different types of pathogens, a bacterial (*Pso*; this project) and the fungal pathogen *Magnaporthe* (33, 34) and minor differences in sampling time periods (Fig. 3). About 43.3% (286/660 genes) of *HAC701*

mutant-DEGs in *Pso* were overlapped with BTH (Benzothiadiazole)-responsive genes (*i.e*. BTH is a synthetic analog of salicylic acid, SA) (Fig. 3A; Table S5; Table S7), while about 12.4% (82/660 genes) of the *HAC701* mutant-DEGs in *Pso* were overlapped with BTH- and WRKY45-regulated genes (Fig. 3B; Table S8). In addition, genes upregulated in plants expressing DEX-induced myc-tagged WRKY45 protein in rice were mostly found in *HAC701* mutant-DEGs in *Pso* (75% or 9/12 genes; Table S9). Our analysis also showed that at most 9.1 % (60/660 genes) of the *HAC701* mutant-DEGs in *Pso* were regulated in BTH- and NPR1-dependent manner (Fig. 3B; Table S10). We then analyzed the 72 *HAC701* mutant-DEGs in *Pso* that were exclusively regulated by BTH- and WRKY45 as well as the other 10 genes jointly regulated by WRKY45 and NPR1 under BTH treatment (Figure 3B-D). We found that most of these *HAC701* mutant genes were genuine WRKY45-regulated genes (Fig. 3C-D) (33, 34). Analysis of these WRKY45-dependent defense-related genes showed that in the presence of *Pso*-infection, number of glutathione-S-transferase (GST) gene, were more upregulated in 9-WT than in *hac701* (Fig. 3D). These results were also consistent with the result that *OsWRKY62*, a known negative regulator and direct target of *OsWRKY45* (34), had lower transcription level in *HAC701* mutants (Fig. 3D). It is interesting that genes in JA biosynthesis, signaling and perception tend to be more highly expressed in *HAC701* mutant than 9-WT (Fig. 3D). In addition, *HAC701* mutant genes that were found regulated in BTH and *WRKY45* indeed contain W-box motifs (35), raising more the possibility that these genes are direct WRKY45 targets (72/82 or 87.8%; Table S11). Meanwhile, all 10 genes that were commonly regulated in BTH, *WRKY45*, and *NPR1* (Fig. 3) contain W-box motifs as well (10/10 or 100%; Table S12). Taken together, these results indicate that upregulation of *WRKY45* as an outcome of *HAC701* mutation resulted in expression profile of genes almost identical to overexpressing *WRKY45* transgenic lines as well as to DEX-inducible *WRKY45* expression system. These also suggest that a significant

fraction of *HAC701* mutant differentially expressed genes (DEGs) are probably WRKY45-targeted, given the presence of W-box motif.

The upregulation of *WRKY45* in *hac701* did not result in any visible morphological defects (Fig. S2G). Previous studies showed that *WRKY45-ox* had no obvious autoimmunity phenotype, although there was a slight decrease in height observed as compared to wild type in response to growth conditions (33, 34). In this study, WRKY45-dependent resistance against *Pso* was observed in *hac701* (Fig. 1D, Fig. S3). Furthermore, these *HAC701* mutants also showed resistant tendencies against *Magnaporthe* infection (Fig. 1E). *WRKY45-ox* treated with *Magnaporthe* showed resistance, while a BTH-induction in knockdown *WRKY45* mutants did not rescue the *Magnaporthe* resistance and remained susceptible (34). Together these results suggest that morphological and disease phenotypes of *hac701* resembled that of *WRKY45-ox* indicating that *HAC701* mutation indeed upregulates *WRKY45* gene that prompts WRKY45-dependent defense pathway into action leading to resistance against bacterial and fungal pathogens.

WRKY45 promoter contains CRE motif.

Rice HAC701 and two others, HAC703 and HAC704, belong to the CBP [Cyclic adenosine monophosphate response element-binding protein (CREB) Binding Protein] family group of proteins that is known to bind CREB transcription factor through its KIX domain (7, 36). Therefore, we examined *in silico* the members of rice CBP family for the presence of KIX domains using a KIX domain database (37). Our results showed that only HAC701 and HAC703 proteins contain the highly conserved KIX domain (Fig. S8). Although we have not identified CREB transcription factor candidate in rice so far, we further examined whether *WRKY45* promoter contains CRE motif that could possibly be targeted via KIX domain and CREB transcription factor-dependent regulation. To our surprise, we found a full CRE motif

within 1 kb upstream of the start codon of *WRKY45* locus (Fig. S9A). Furthermore, we checked the occurrence of CRE motif in *hac701* DEGs during infection and found that only five genes including *WRKY45* (0.76%) contain full CRE motif (Fig. S9; Table S5). These data show that *WRKY45* promoter could possibly be *cis*-regulated by HAC701 through its KIX domain, while the occurrence of CRE motif is not necessarily associated with other HAC701-regulated genes.

Genome-wide investigation of histone modifications and enriched gene targets in *HAC701* mutant.

The CREB-binding protein (CBP) is also known to regulate gene expression by acetylating histone tails in both animals and plants (38). Thus, we performed chromatin immunoprecipitation coupled to sequencing (ChIP-seq) analysis on histone markers associated with active and repressive chromatin to examine the landscape of chromatin modifications in *HAC701* mutant. We performed ChIP-seq analyses of H3K9 acetylation (H3K9ac), H3K27 acetylation (H3K27ac), H3K9 di-methylation (H3K9me2), and H3K9 tri-methylation (H3K9me3) on 9-WT and *9-12b*$^{-/-}$ mutant (Fig. S10; Table S13). Metaplot profiles of these histone modifications were generated for genes, transposable elements (TEs), and simple repeats (Fig. S11; Fig. S12). The enrichment profiles show that both H3K9ac and H3K27ac accumulated in genes mainly along the transcriptional start site (TSS) and tapering through the gene body regions. In contrast, we found that H3K9me2 and H3K9me3 were highly depleted in the gene TSS region (Fig. S11A). As expected, H3K9 and H3K27 acetylation marks were depleted in TEs, while H3K9 di- and tri-methylation marks showed enrichment (Fig. S11B). In addition, enrichment analysis of simple repeats showed similar profiles with TEs in both acetylation and methylation histone marks, although simple repeats tend to be highly enriched in H3K9me2 at a narrow set of genomic loci (Fig. S12).

These results showed that our ChIP-seq profiles of histone modifications were largely consistent with the previous report on rice ChIP-seq analysis (39).

The observed low enrichment of H3K9ac in *9-12b*$^{-/-}$ mutant is a probable indication of mutation on *HAC701* gene (Fig. S11A). Therefore, we further analyzed the significantly enriched or depleted regions in *9-12b*$^{-/-}$ by taking the enrichment ratio of 9-WT over *9-12b*$^{-/-}$ (wild type/*hac701*) in H3K9ac, H3K27ac, H3K9me2, and H3K9me3 modifications. We found that H3K9ac fraction yielded peaks (265 regions) (Fig. 4A; Table S13). From the metaplot analysis, it showed that *9-12b*$^{-/-}$ has depleted H3K9ac enrichment in the 265 regions identified containing putatively 263 genes (Fig. 4A; Table S14), which include *HAC704* and *HAC701* loci and a mediator gene, *MED11* (Fig. 4D; Fig. S13A). These 265 regions were not associated with changes in other modifications in *9-12b-/-* mutant when compared to 9-WT (Fig. 4B). These results suggest that HAC701 acetyltransferase may have a specificity to H3K9 site. It also suggests that HAC701 probably autoacetylates its own promoter including another member of CBP family, *HAC704*.

We then analyzed the GO enrichment features of the putative 263 genes found in these 265 regions with H3K9ac changes (Fig. 4C; Table S14). The results indicate that these genes function in processes involved in the flow of genetic information, DNA methylation in the CHH-context, circadian rhythm, organellar transport, cell cycle and reproduction, ubiquitination, and in a number of biosynthetic processes. It is also perhaps not surprising that histone acetylation was also enriched. In addition, enrichment of genes involving environmental responses included heat stress and innate immunity were observed, in which about 9% (23/263) were possibly involved in defense responses. A large fraction of these defense genes were identified as candidate sensors or decoys (e.g. Cyclin A1, Thioredoxin, Jacalin-like lectin, *etc.*) that may act as negative regulators of rice effector-triggered immunity (ETI-immunity) (40) (Fig. 4E; Fig. S13B). The distribution of these 265 regions in

H3K9ac ChIP revealed that a large portion were found in genes (73.58%) followed by promoters (18.11%) (Fig. S14). It is also interesting to note that H3K9ac in these identified regions was found in transposable elements (7.55%). Overall, these results demonstrate that HAC701-dependent acetylation of H3K9 histone site might modulate transcription of decoy genes that are monitored by NLR proteins in rice immunity. Additionally, H3K9ac assessed in different regions of the rice genome showed that it is found mostly in genes and promoters with high similarity in the previous study (39).

We proceeded by analyzing the general distribution of H3K9ac, H3K27ac, H3K9me2, and H3K9me3 peaks in intergenic and intragenic regions of rice genome in 9-WT and *9-12b*$^{-/-}$ mutant (Fig. 5A). A large proportion of H3K9ac and H3K27ac were concentrated on exonic and intronic regions of the gene, while *HAC701* mutation resulted in the increase of enrichment of H3K27ac genome-wide on all regions of the rice genome (Fig. 5A). It is also worth mentioning that loss of *HAC701* increased the level of enrichment of these methylation modifications in intergenic regions. These data suggest that the loss of *HAC701* leads to an increase of a counter acetylation modification, H3K27ac, on a genome-wide scale.

To explain the disease resistance phenotype of *hac701* through WRK45-dependent immune pathway, we investigated the genomic locus of rice *WRKY45* (Fig. 5B). The upregulation of WRKY45 was accompanied by H3K9ac enrichment along the 1kb upstream region of *WRKY45* gene in *9-12b*$^{-/-}$ (Fig. 5B, C). As the CRE motif was specifically enriched in the promoter region of *WRKY45* (Fig. S9A), we compared the enrichment of H3K9ac and H3K27ac in *9-12b*$^{-/-}$ *WRKY45* promoter. We found that H3K9ac, but not H3K27ac, was highly enriched in this regulatory region (Fig. S15), while H3K27ac of *WRKY45* gene body was less pronounced than H3K9ac. Overall, our ChIP-seq data are consistent with RNA-seq data in showing that mutation in *HAC701* gene potentiated *WRKY45* locus by regulating the enrichments of histone acetylation and methylation modifications on *WRKY45* promoter. We

also found that the CRE motif of *WRKY45* is modulated by H3K9ac and perhaps other modifications, including those that are analyzed here.

Systemic gene expression in rice-*Pso* pathosystem. To explore the nature of systemic gene expression in rice-*Pso* pathosystem, we performed RNA-sequencing on systemic or distal tissues of 9-WT and *hac701* plants. The tissue samples were collected together with infected samples (local samples) 72 hours after *Pso* infection without further bacterial treatment. Genome-wide transcriptome analysis in systemic 9-WT samples showed that 24 genes were differentially expressed, and among them were eight genes that were common to both local and systemic tissues (Fig. S18A; Table S16). Comparative analysis also showed that although there were substantial expression changes in systemic tissues, the number of DEGs was highly reduced in systemic tissues than in local tissues. Among the eight DEGs, five of them showed altered transcriptional expression from local to systemic tissues (Fig. S18B). These genes were mannose-specific jacalin-related lectin/*OsJAC1* (Os12g0247700) (41), putative cytochrome P450 (Os09g0275400), ATPase (Os07g0187400), GDP-L-galactose phosphorylase (Os12g0190000), and terpene synthase (Os04g0344100), some with putative functions in response to pathogen infection or stress. These results indicate that these genes were mostly activated locally in the infection site and that any altered expression in distal tissues may facilitate systemic form of resistance. To compare the effect of *HAC701* mutation on the number of DEGs, we analyzed the MA-plots of systemic tissues of 9-WT and *hac701*. Our results showed that the number of DEGs with significant expression (*i.e.* those that are in red) was diminished in the mutant background implicating a possible role of *HAC701* in systemic signaling in rice-*Pso* pathosystem (Fig. S19). Overall, these results indicate that systemic tissues in *Pso*-challenged 9-WT plants have augmented transcriptional gene expression that possibly aims to 'prime' distal tissues on the onset of secondary pathogen attack. This also indicates that *HAC701* might potentially regulate systemic defenses through

an unknown mechanism at distal non-infected site in preparation for future infection episodes.

DISCUSSION

Histone acetyltransferases or HATs and their complexes are involved in various biological processes in the cell. Currently, studies have been focused on the roles of HATs specifically members of the CREB-binding protein (CBP) family in regulating substrate specificity and enzymatic activity such as acetylation (38). However, its involvement in molecular signaling pathway leading to modulation of plant immunity remains to be explored. Therefore, it is expected that the analysis of plant CBP will facilitate a broader understanding of regulation of gene expression and protein function in plant immunity pathways.

In this study, we generated CRISPR/Cas9 mutants of the rice *HAC701* gene, a member of the CBP family of HATs, since our results indicated its involvement in rice immunity. By inoculating a rice compatible bacterial pathogen, *Pseudomonas syringae* pv. *oryzae* (*Pso*), we showed that *hac701* are resistant to *Pso* proliferation and also showed resistance tendency when infected with *Magnaporthe* (rice blast). These indicates that *HAC701* negatively regulates rice immunity responses to *Pso* and *Magnaporthe* pathogens. When we analyzed our transcriptome data, it showed that this negative regulation of immunity by *HAC701* is attributable to suppression of a major immunity pathway in rice probably through WRKY45. In *hac701*, *WRKY45* gene expression is upregulated and it seemed to be in a primed state enabling a further increase of expression upon bacterial infection. In addition, both morphological phenotypes and target genes in *hac701* mimic those in *WRKY45-ox* transgenic lines possibly indicating a genetic interaction of *HAC701* and *WRKY45* genes. Lastly, we showed in our ChIP-seq analysis that the promoter of *WRKY45* in

hac701 is enriched in H3K9ac coinciding with a *cis* regulatory CRE motif that might be responsible for *WRKY45* upregulation and control.

In Arabidopsis, the p300/CBP acetyltransferase gene, *HAC1*, has been shown to positively regulate defense priming only in repetitively abiotic-stressed plants (42). *hac1-1* did not show any immunity related responses prior to abiotic stress applications indicating that Arabidopsis *HAC1* requires several abiotic stress stimulations to activate its immunity. However, this is not the case in *HAC701* in rice. We showed that the rice *HAC701* did not need abiotic stress stimulation to be transcribed and to effect pathogen and disease specific phenotypes (Fig. S1; Fig. 1D-E; Fig. S3). Rather, our results are consistent with the disease phenotype exhibited by Arabidopsis mutant of GCN5, an acetyltransferase member of the SAGA transcriptional coactivator complex catalyzing the H3K14 modification site and at the same time influencing the acetylation of H3K9 (43). The *gcn5* showed upregulation of SA-mediated immunity resulting in resistance against *Pseudomonas syringae* pv. *tomato* infection. In our study, we found that WRKY45-dependent pathway confers resistance to *hac701*. Consistent with the view that the rice hormone defense network does not support a dichotomous role of salicylic acid (SA) and jasmonic acid/ethylene (JA/ET) phytohormones in regulating rice immunity (44), we found no evidence in this study that SA-mediated immunity played a central role in *hac701* resistance phenotype. However, we found JA-related differential gene expression as components of WRKY45-dependent defense-related genes (Fig. 3D). Indeed, JA biosynthesis is known as a downstream target of rice WRKY45 (45). In rice immunity model, both SA and JA/ET are considered effective in defense responses against (hemi) biotrophic and necrotrophic pathogens (44, 46, 47). While SA-mediated *AtNPR1* regulates majority, if not all, of Arabidopsis immune responses (48), *OsWRKY45* and *OsNPR1/NH1* are mostly independent of each other (34; Fig. S26). Although, our results suggest that *hac701* DEGs partially overlapped with NPR1-dependent

pathways (Fig. 3B). Given that the rice system has a constitutive high levels of SA compared to most plants including Arabidopsis and tobacco, and pathogen applications did not increase its basal SA level (49, 50), our results are consistent with this report that SA in rice may not directly act on pathogens, rather, it may function to prime endogenous defense pathways in which *WRKY45* plays the central role. *OsWRKY45-ox* showed strong resistance against blast pathogen, even though lacking the constitutive expression of defense genes prior to blast infection (34). It could be that disruption of HAC701-dependent pathways through *HAC701* mutation led to activation of WRKY45-dependent pathways in an already SA-primed rice network. But, this needs to be further examined in detail. Our results are also consistent with the disease phenotype presented by non-sense mutation in *Med15* gene, a subunit of Mediator complex (51). The *med15b.D* wheat mutants were resistant to stem rust, and the authors attribute a part of this to segmental coregulation in which a certain portion of the chromosome containing NLR genes was differentially expressed in wild type compared to mutant. While we did not observe any form of segmental coregulation in our analysis of *hac701*, we found that mutations in *HAC701* resulted in downregulation of ETI components notably the decoys/sensors (Fig. 4E).

OsHAC701, *AtHAC1*, *AtGCN5*, and *TaMed15*, play a central role in regulating the transcriptional machinery. They likely do this regulation by associating themselves and their complexes to RNA polymerase II and transcription factors as shown by their homologous counterparts in animals (4, 14, 52, 53). This is possible because they are multidomain genes that have the capacity to form and maintain large complexes. Os*HAC701*, *AtHAC1*, and *AtGCN5* are also involved in regulating abiotic stress responses suggesting that the complexity and specificity of their activities are dependent on their interacting factors that recruit them to the biological pathway itself (6, 7). Furthermore, majority of these genes,

OsHAC701, *AtHAC1*, and *TaMed15*, encode the KIX domain, a docking site for transcription factors reported to be involved in plant immunity (54).

In line with the above results, we propose that HAC701 is a negative regulator of WRKY45-dependent defense pathway in rice (Fig. S20). We suggest here two possible mechanistic insights into HAC701 regulation of WRKY45 that need further experimental evidence. First, similar to Med15, the HAC701-mediated immunity may require a loss or truncation of HAC701 in regulating the transcription of *WRK45* locus. Given that the promoter of *WRKY45* contains a rare CRE motif (Fig. S9), we assume that an unidentified CREB-like transcription factor with regulatory potential is interacting with HAC701 through its KIX domain (Fig. S8) and with the CRE motif of *WRKY45* promoter. This interaction may also include other protein interactors specific to *WRKY45* locus regulation. From our results, mutation of *HAC701* is enough to prime *WRKY45* and further addition of *Pso* enables *hac701* to mount higher *WRKY45* transcription compared to 9-WT. These suggest to us that *WRKY45* locus is poised for activation as suggested by our ChIP-seq analysis of untreated *hac701* (Fig. 5). The H3K9 acetylation we observed might not be catalyzed by HAC701, but may come from other CBP family members (Fig. 1A) or other HATs. Although, we do not have ChIP-seq data for pathogen inoculated *hac701*, our RNA-seq data suggest that the poised *WRKY45* through *HAC701* mutation is enough to activate downstream defense likely through *WRK45*-dependent signaling. Second, the decoys/sensors component that we found may act as negative regulators as predicted by the Decoy model (Fig. 4E) (40, 55). It could be that HAC701 maintains the acetylation of these decoys/sensors to equilibrium. Any disturbance in their expression could possibly lead to activation of R genes monitoring these decoys/sensors, which could in effect activate WRKY45-dependent immunity. Indeed, we found seven R genes upregulated in *HAC701* mutation treated with *Pso* (Table S17). It is of course possible

that these two mechanisms are occurring simultaneously in conferring resistance, although finer details of these mechanisms are still unknown.

The heterochromatic marker, H3K9me3, is common in animals, but rarely found in Arabidopsis and in plants in general (56). Indeed, our analysis did not find the peaks in 9-WT ChIP-seq, although we found 33 peaks in the *HAC701* mutant (Table S15). Most H3K9me3 enrichments were found in intergenic regions and in only two genes with intragenic enrichments. Table S15 also shows genes nearest the H3K9me3 enrichment in the intergenic regions. These results suggest that H3K9me3 is may be a rare modification and is possibly modulated by HAC701 presence and activity in certain genomic regions.

Trade-off between growth and defense in plants is a common occurrence and often considered inevitable (57, 58). However, we were surprised to find that *hac701* in the T2 up until T4 generations do not have readily visible penalty yields (*e.g.* number of effective grains and grain weight) (Fig. S2F-H). It could be that the primed state of *WRKY45* in *hac701* has modulated the expression of resistance from affecting these agronomic traits. Nonetheless, the mechanistic basis for this trade-off, if it truly exists, is not well understood and needs further investigation.

We would like to emphasize that at the moment we do not have strong evidence that HAC701 specifically catalyzes H3K9 acetylation. Although, the H3K9ac antibody used in this study detected H3K9ac decrease of numerous loci in *hac701* compared to 9-WT that are not present in H3K27ac, histone target-specificity of HAC701 still needs to be verified. As H3K9ac and H3K14ac were seemed co-regulated and were directly correlated to each other in regulating their common target genes (43), we assume that the H3K14ac in our *hac701* would show the same correlation as well.

HAC701 appears to be an ancient protein in the CBP histone acetyltransferase family clade (Fig. 1A). The fact that *HAC701* mutation is not lethal, suggests that other CBP members and arguably members of other histone acetyltransferase families might have redundant functions at some regulatory level. However, our results that *hac701* showed enhanced disease resistance phenotype and reduction in acetylation demonstrate certain functional specificities through HAC701-dependent pathways. Also, the fact that *hac701* showed reduction in expressed genes at the systemic level (Fig. S19), indicates possible broader roles of HAC701 other than localized modulation of rice innate immunity.

MATERIALS AND METHODS

Biological samples and plant growth conditions. *Oryza sativa* ssp. *japonica* cv. Nipponbare (wild type) plants and mutant lines were grown in commercial soil (Kumiai, JA Okinawa) at 30°C day/25°C night temperatures under a 12-h-light/12-h-dark photoperiod in an incubator (BiOTRON, NK System). The lighting was supplied by white light at an intensity of 31,000 lx. Relative humidity was at 70%. For embryonic rescue, rice embryos were extracted from wild-type immature seeds 10-14 days after flowering. Embryos were grown into plantlets in Murashige and Skoog (MS) agar medium before being transferred to soil for further growth.

Isolation and screening of *HAC701* mutant lines. To generate *HAC701* CRISPR/Cas9 knockout mutant lines, two sgRNA *HAC701*-specific target sites were obtained from CRISPR-P website and were used to synthesize primers for pRGEB31 (stable system) (59) (Table S1). Briefly, the vectors were digested with BSA I, while primers were phosphorylated and annealed to produce a DNA oligo duplex. The digested vectors were ligated to DNA oligo duplex using T4 ligase. CRISPR/Cas9 vectors were introduced into *Agrobacterium* EHA105 and rice calli were transformed using the standard *Agrobacterium*-

mediated transformation procedure. For CRISPR/Cas9 T0 and T1 screening, leaf samples were collected and genomic DNA was extracted using a standard CTAB protocol. Then, PCR-RFLP assay utilizing BseLI restriction enzyme (Thermo Fisher Scientific) was used to detect the CRISPR/Cas9-engineered mutations on *HAC701* targets (Table S1). Positive lines detected by PCR-RFLP assay were further analyzed by sequencing for INDEL mutations using S2 and S5 forward primers (Table S1). Four DNA amplicons per line were cloned and sequenced to determine the zygosity of the lines. Biallelic mutations were found in a few T0 and T1 lines. First exon (Target 1) was initially targeted in *HAC701* gene using a CRISPR/Cas9 vector construct containing a single-guided RNA (S2) (Fig. S2A; Table S1). The isolation of the first generation (T0) *CRISPR Cas9-HAC701-S2* lines yielded 90 positive independent lines, and among these, randomly chosen representative lines were further genotyped to characterize the identified DNA mutation. PCR and RFLP assays resulted in the isolation of monoallelic lines characterized mostly by deletions and a few insertions (INDELS) on or surrounding the targeted site of sgRNA (S2) (Fig. S2B-C; Table S1). The T1 *HAC701-S2* generation as observed from seeds showed conservation of mutation directly from parental lines (Fig. S2B). Then, mutant lines were isolated using the same technology targeting the fifth exon (Target 2) of the *HAC701* gene using a construct that also contains a single guide RNA (S5) (Fig. S2D; Table S1). The *CRISPR-Cas9-HAC701-S5* (T0) lines generated 11 positive independent lines of which three were genotyped for verification of mutations (Fig. S2E). Second generation (T1) lines also showed conservation of mutations (Fig. S2E). Similar to *HAC701-S2* lines, genotyping showed INDELS in proximity to or on the target site.

Phenotyping. Positive lines containing biallelic homozygous mutations were phenotyped for effective grain production by examining and counting the mature grains produced in each panicle. Tiller number was counted one month after flowering. Chlorosis phenotype was used

as a proxy for any defect in photosynthesis and or apparatus. 1000-grain weight was measured on seeds oven dried for 30-days at 37°C. Comparison of height and general morphological structures were documented using photography.

flg22 leaf disc assay. flg22 peptide, a well-known inducer of plant innate immunity, specifically of PTI was used to test which rice HATs respond to flg22 treatment. Leaf disc assay (modified from 60, 61) was performed on fully expanded 30-d-old wild-type leaf samples and treated with synthetic flg22 peptide (30-51 aa, Flic, *Pseudomonas aeruginosa*) (ADI, Inc.) at different time periods and concentrations. Briefly, leaves were cut into about 5 mm sizes and floated on the water for 24-h in growth chamber to remove the symptoms of wounding stress. Leaves were then treated with PAMP solution in water at 15 ml falcon tubes with rotation (Corning Science). After treatment, paper towel-dried leaves were frozen in liquid nitrogen.

Pathogenesis assay. Seeds were surface sterilized and imbibed in sterile water in the dark for 72 h before sowing on MS basal medium (Sigma Life Science). After 10 days, the plantlets were transferred to soil and were grown for another 18 days until infection. *Pseudomonas syringae* pv. *oryzae* (*Pso*) (MAFF No. 301530, NIAS Genebank) was grown in Luria-Bertani (LB) broth (Sigma-Aldrich) at 28°C until OD = 0.2 and was resuspended in 10 mM $MgCl_2$. The fourth leaf counting from the first true leaf was infected with *Pso* using needleless syringe injected from the lower surface of the leaf. *Pso* leaf infiltration was performed 10 cm from the tip of the leaf and was done 3x with approximately 1 cm space between the infiltration sites. Infected plants were temporarily maintained outside the growth chamber for 2 h to allow drying of the infected sites before returning to the chamber. Infected leaf samples were collected 3 days after *Pso* inoculation utilizing only the tissues comprising the spaces between the infiltration sites. These tissues were grounded in sterile 10 mM $MgCl_2$ and the grounded tissue suspensions were transferred to LB agar medium for incubation. The

infected local tissues were assayed with minor modifications as detailed in Liu, *et al*. (62). For log cfu per leaf disc measurement, the grounded tissue suspensions were serially diluted six times to be able to count with accuracy the *Pso* colonies on Luria-Bertani (LB) agar medium. *Pso* colonies were counted from 4th until 6th serial dilution in several independent and genotypically dissimilar *hac701* lines, *9-12b*$^{-/-}$, *9-5*$^{-/}$, and *9-12a*$^{-/-}$. The remaining samples of the fourth leaf were used for RNA-sequencing analysis. For blast assay, the fifth leaf of 25-day-old plants were used for infection of *Magnaporthe oryzae* (MAFF No. 101511, NIAS Genebank). Blast spores were incubated 10 cm from the tip of the leaf (1st site) and at another site of the same leaf 10 cm from the first site (2nd site). Infected plants were incubated for 10 days inside an incubator (BiOTRON, NK System) and the length of blast infection was measured.

Gene expression analysis. Total RNA extraction was performed using RNeasy Plant Mini Kit (Qiagen) or Maxwell® 16 LEV Plant RNA Kit (Promega). cDNA was synthesized using Primescript II 1st Strand cDNA Synthesis Kit (Takara) according to manufacturer's instructions. RT-qPCR assays were performed on three biologically independent samples or as indicated. RT-qPCR was performed using SYBR Premix Ex Taq II (Tli RNaseH Plus) (Takara) and was calculated following Pfaffl (63) by averaging the values relative to *ACT1* control gene. Primer sequences are listed in Table S18.

RNA-sequencing. Total RNA was isolated from mock- and *Pseudomonas syringae* pv. *oryzae* (*Pso*)-treated 9-WT wild type and *hac701* with Maxwell 16 LEV Plant RNA Kit (Promega) run on the Maxwell 16 Instrument (Promega) and/or mirVana miRNA Isolation Kit (Invitrogen by Thermo Fisher Scientific). The *hac701* lines, *9-12b*$^{-/-}$ and *9-5*$^{-/-}$, were lumped together as two independent biological samples during analysis. To remove the contaminating genomic DNA from RNA samples isolated using the mirVana miRNA Isolation Kit, RNA was treated with DNase I (RNA free) (Nippon Gene) following the

manufacturer's instructions. Samples were submitted to OIST Sequencing Center for RNA quality checking, library preparation, and paired-end mRNA-sequencing (PE mRNA-seq).

Chromatin immunoprecipitation-sequencing.

ChIP analysis of histone modifications in wild type and mutants were performed as follows: One-month-old mature leaves of wild type (9-WT) and *hac701* (*9-12b*$^{-/-}$) mutant were fixed in a fixation buffer (10mM Tris-HCl (pH 7.5), 50 mM NaCl, 0.1 M sucrose, 1 % formaldehyde) for 10 min, followed by quenching by 125 mM Glycine for 5min. Nuclei isolation was performed as previously described (64). Immuno-precipitation was performed for two replicates for each genotype (about 1 g tissue/IP) by SimpleChIP Plus Kit (Cell Singaling Technology) according to the manufacturer's instructions. Anti-Histone H3 antibody (Abcam ab1791), Anti-acetyl Histone H3K9 antibody (Merck ABE18), Anti-Dimethyl Histone H3K9 antibody (Merck 05-1249), Anti-Trimethyl Histone H3K9 antibody (Merck 17-10242), Anti-acetyl Histone H3K27 antibody (Abcam ab4729) were used for IPs. Dynabeads M-280 Sheep Anti-Rabbit IgG (Invitrogen 11203D) or Anti-Mouse IgG (Invitrogen 11201D) was used for purification of chromatin-antibody complex. Precipitated DNA samples were sequenced by Hiseq 4000 in 150 bp paired-end mode in OIST Sequencing Center. For ChIP real-time PCR, we used the "Percent Input Method" (Thermo Fisher Scientific) with 33% input value to normalize the data for enrichment calculation. Three independent biological replicates were performed for each sample.

Data analysis. For RNA-sequencing analysis, high quality reads were trimmed in order to remove sequencing bias and adapter effects. Trimmed reads were then mapped to the *Oryza sativa* spp. *japonica* genome (Os-Nipponbare-Reference-IRGSP-1.0) using Tophat (65, 66). Custom R scripts were used to generate the RNA count table necessary to analyze the differentially expressed genes (DEGs). Differential expression analysis was performed using

DESeq2 package involving count normalization, dispersion estimation, and differential expression test (67). DEGs were selected at Benjamini-Hochberg adjusted *p* value of < 0.01. To perform Gene Ontology (GO) analysis, gene lists were submitted to Enrichment Analysis (68) web tool of the Gene Ontology Consortium (69-71). To create the Venn diagram, gene sets were submitted to InteractiVenn web tool using *unions by list* to obtain overlapping components of input datasets (72). For ChIP-sequencing analysis, raw reads were trimmed and were mapped to *Oryza sativa* spp. *japonica* genome (Os-Nipponbare-Reference-IRGSP-1.0) using Bowtie (73). Read alignments were visualized using Integrated Genome Browser (IGB) (74). ChIP-enriched peaks were called by deriving a quantitative reproducibility score called "irreproducibility discovery rate" (IDR) (68). Comparative analyses and quantitation of enrichments between 9-WT and *hac701* (*9-12b*$^{-/-}$) were analyzed using a suite of tools and utilities found in deepTools (75) and BEDTools (76). Peaks were positioned to genomic locations (intergenic, genes, transposable elements, simple repeats) and within genes (promoter, exon, intron, TSS, TTS). Table S13 showed the number of peaks identified for each histone modifications in 9-WT and *hac701* (*9-12b*$^{-/-}$). Peak-to-gene assignment was performed using Homer (v4.11) (77). To create the phylogenetic tree of Arabidopsis and rice histone acetyltransferases, we used the UniProt amino acid sequences and reconstructed the phylogenetic relationships using Phylogeny.fr (78, 79). For KIX domain analysis, we used KIXBASE to perform multiple sequence alignment (37). To identify *cis*-elements on DNA sequences, we used cister prediction software that utilizes hidden Markov model (80).

Data visualization. Visualization of majority of the data was performed using Microsoft Excel for Mac 2011 (version 14.7.1) and R packages: heatmaply, functions from *gplots*, and *ggplot2*.

Data Repository. For RNA-sequencing and ChIP-sequencing, raw data will be deposited shortly in the DDBJ Sequence Read Archive. Processed data will also be deposited in

"Epigenomics Data site" maintained by Plant Epigenetics Unit (https://plantepigenetics.oist.jp/). All other data can be found in the Supplemental Tables 1-18 in this manuscript.

FIGURE LEGENDS

Figure 1 Disease phenotype of biallelic homozygous CRISPR/Cas9 lines targeting the fifth exon of rice acetyltransferase gene, *HAC701*. (*A*) Phylogenetic relationships of members of Arabidopsis and rice histone acetyltransferases. The numbers in red are branch support values. All amino acid sequences are from UniProt database. (*B*) Upper panel: Alleles from four lines of the second generation (T1) plants were identified by cloning and sequencing the PCR products from *HAC701* target region using the primers found in Table S1. Lower panel: PCR and RFLP assays of representative T1 generation lines. The mutant line *9-12a*$^{-/-}$ displaying a wild type-like band was due to unaltered sequence order recognized by BseLI even after an insertion event, however we confirmed by sequencing that an insertion mutation was present in this line. (*C*) *Pseudomonas syringae* pv. *oryzae* (*Pso*) infection assay of *hac701*, *9-12b*$^{-/-}$ and *9-5*$^{-/-}$ (T2), using *9-5*$^{+/+}$ segregated wild type line (9-WT) as control. Bacterial density quantification uses values from 4th-6th serial dilutions. The mutant line *9-12b*$^{-/-}$ was grown from the seeds of the third generation (T2), while *9-5*$^{-/-}$ line was embryonically rescued about 15 days post flowering from the second generation (T1) parental plants. All mock measurements yielded zero bacterial growth for both wild type and mutant lines. Bars represent the 95% confidence interval (CI) and compared to the wild type using two-tailed Student's *t*-test at $P<0.05$ in *9-12b*$^{-/-}$; one-tailed Student's *t*-test at $P<0.05$ in *9-5*$^{-/-}$. (*D*) *Magnaporthe oryzae* infection assay of *hac701*, *9-12b*$^{-/-}$ and *9-5*$^{-/-}$, using *9-5*$^{+/+}$ segregated wild type line (9-WT) as control. Lesion length was measured on leaves after 10 dpi (days post infection). White length indicator bar on the left panel is 10 mm. Bars on the

right panel represent standard error (SE) and compared to the wild type using *F*-test for variance and Student's *t*-test.

Figure 2 The rice *WRK45* gene expression is induced in *hac701* lines. (*A*) Overlap analysis of upregulated and downregulated genes in *hac701* background under mock and pathogen (*Pso*)-treatment conditions. *OsWRKY45* is the only differentially expressed gene in either the absence or presence of pathogen. Transcriptome data were normalized using mock data sets for each genotype and condition. (*B*) *OsWRKY45* expression when *HAC701* is mutated (+ sign). The addition of pathogen (+ sign) on *hac701* increased further the *OsWRKY45* expression. Transcriptome data of *hac701*, *9-12b*$^{-/-}$ and *9-5*$^{-/-}$, under mock or *Pso*-treated conditions were lumped as two independent biological samples for analysis (See Table S2). hpi, hours after infection.

Figure 3 *hac701* phenocopies *OsWRKY45* overexpression transgenic plants. (*A*) Overlap analysis of differentially expressed genes (DEGs) in *hac701* background with benzothiadiazole (BTH)-responsive genes (*i.e.* BTH is a salicylic acid analog) in wild type rice. (*B*) Overlap analysis of DEGs in *hac701* background with BTH-inducible and *OsWRKY45*-dependent or *OsNPR1*-dependent genes. (*C*) *OsWRKY45*-dependent defense pathway components. (*D*) Gene expression of *OsWRKY45*-dependent defense genes in 9-WT and *hac701*.

Figure 4 Genome-wide H3K9 acetylation is depleted in *hac701*. (*A*) Heatmap showing the accumulation of H3K9 acetylation on 265 peaks by taking the enrichment ratio of 9-WT and

9-12b$^{-/-}$ data (Wild type/mutant). (*B*) Heatmaps showing the accumulation of H3K27 acetylation, H3K9 di-methylation, and H3K9 tri-methylation on 265 peaks by taking the same enrichment ratio as (*A*). Heatmaps in (*A*) and (*B*) are representatives of two biologically independent data showing similar enrichment results and number of peaks identified. (*C*) GO enrichment analysis showing only the "Biological Process" of the 263 genes found in the 265 peaks. Numbers in enrichment indicate Fold Enrichment Value using Fisher's Exact test with results for uncorrected $P<0.05$. (*D*) Enrichment scores of seven representative genes showing depletion of H3K9 acetylation in *hac701*, *9-12b*$^{-/-}$. (*E*) Enrichment scores of 10 representative putative decoy/sensor genes (40) showing depletion of H3K9 acetylation in *hac701*, *9-12b*$^{-/-}$. Scores in (*D*) and (*E*) are averages of two biologically independent samples with bars showing standard deviation (SD).

Figure 5 *OsWRKY45* loci is enriched in H3K9 acetylation in *hac701*. (*A*) Enriched peaks on histone modifications positioned to genomic locations (Intergenic, Promoter-TSS, Exon, Intron, and TTS) in 9-WT and *hac701*, *9-12b*$^{-/-}$. All data were normalized to input. (*B*) *OsWRKY45* depth graph of RNA-seq and H3K9 acetylation ChIP-seq showing the number of reads in RPKM (Reads Per Kilobase of transcript, per Million mapped reads) in 9-WT and *hac701*. The red dotted box shows the 1kb upstream region of *OsWRKY45* with arrow indicating the direction of transcription. (*C*) Upper panel: Gene map of *OsWRKY45* with arrow showing the direction of transcription, gray bars are 5' and 3' untranslated regions (UTRs), black bars are exons, and white bars are introns. Lower panel: 9-WT and *hac701* (*9-12b*$^{-/-}$) mutant ChIP-qPCR showing enrichments of H3K9 acetylation and H3K9 di-methylation in *OsWRKY45* locus. The significant difference in enrichment is computed using two-tailed Student's *t*-test where asterisks: ***$P<0.01$, **$P<0.05$, and NS means Not Significant.

TABLE LEGENDS

None

SUPPLEMENTARY FIGURE LEGENDS

Figure S1 Characterization of mutations generated by CRISPR/Cas9 editing on the first and fifth exon of rice acetyltransferase gene, *HAC701*. (*A*) Schematic showing an sgRNA targeted to the first exon of *HAC701* gene. (*B*) PCR and RFLP assays of representative T0 and T1 generation lines from leaf blade (Lb), panicle (Pa), and seed (S) DNA samples. +/+ and M represent the zygosity of the line, where +/+ refers to wild type and M refers to monoallelic. (*C*) Alleles from 12 T0 generation lines identified by cloning and sequencing the PCR products from *HAC701* target regions using the primers found in Table S1. Similar line number indicates that lines came from the same callus. For each line, four DNA amplicons were cloned and sequenced and the fraction indicates the number of times the type of mutations were found in each line. In case not indicated, it means wild type. The asterisk (*) indicates the most common mutation found within and across different lines. (*D*) Upper panel: Schematic showing an sgRNA targeted to the fifth exon of *HAC701*. Lower panel: Schematic showing the protein domains of HAC701. (*E*) PCR and RFLP assays of representative T0 and T1 generation lines from leaf blade DNA samples. +/+, M, B represent the zygosity of the line, where +/+ refers to wild type, M refers to monoallelic, and B refers to biallelic. T1 lines came from parental 2-3 line. (*F*) Phenotype of T2 lines showing effective grains and tiller number. (*G*) Images of T3 *hac701* lines compared to segregated wild type, 9-WT. (*H*) RT-qPCR levels of *HAC703* and *HAC704* genes in *HAC701* mutation line background. Samples were treated hydroponically with HDAC inhibitors (1μM Trichostatin A (TSA) and 100 μM Nicotinamide at final concentration) for three days. Bars represent

standard error (SE); n= 3. The significant difference in transcription is computed using two-tailed Student's *t*-test where asterisks: *$P<0.01$. (*I*) Phenotype of T3 and T4 lines showing grain weight.

Figure S2 flg22 induced the expression of rice pathogenesis-related and histone acetyltransferase (HAT) gene, *HAC701*. Transcriptional levels of pathogenesis-related gene, *PR10a*, and of eight HAT genes upon flg22 induction at concentrations in μM units. Data shown are means ± SE; n= 3. The significant difference in transcription is computed using two-tailed Student's *t*-test where asterisks: ***$P\leq0.01$, **$P\leq0.03$, * $P\leq0.05$.

Figure S3 *Pseudomonas syringae* pv. *oryzae* (*Pso*) infection assay in T2 *hac701* line, *9-12a*$^{-/-}$. Values from 4th-6th serial dilutions were used for quantification. Segregated wild type line was used as a control. Bars represent the 95% confidence interval (CI) and compared to wild type using one-tailed Student's *t*-test at $P<0.05$.

Figure S4 Sample distances of RNA-seq data after regularized-logarithm transformation (rlog). (*A*) Heatmap showing the Euclidean sample distance matrix of mock- and *Pseudomonas syringae* pv. *oryzae* (*Pso*)-treated samples in two biologically independent replicates. (*B*) Principal component analysis (PCA) of the mock- and *Pso*-treated RNA-seq samples. Principal component 1 (PC1) compares the variance between mock- versus *Pso*-treated samples. Principal component 2 (PC2) compares the variance between biological replicates within treatments.

Figure S5 Top 10 genes that are most highly variable in mock- and *Pso*-treated RNA-seq samples. Gene descriptions were derived from Oryzabase: Integrated Rice Science Database (NBRP) and Rice Genome Annotation Project (NSF). Two biologically independent RNA-seq replicates are presented.

Figure S6 Rice-*Pseudomonas syringae* pv. *oryzae* (*Pso*) pathosystem. (*A*) Enriched pathways in the rice-*Pso* pathosystem. (*B*) MA-plot of the rice-*Pso* pathosystem showing log fold changes upon 72 hpi (hours post infection). *P* adjusted value is set at < 0.1. (*C*) Plot dispersion estimates of genes in the rice-*Pso* pathosystem. The red line indicates the trend showing the dispersion's dependence on the mean. The blue points are the final estimate of each gene in reference to the red line. The blue circles are genes with high gene-wise dispersion estimates and are considered outliers. Two biologically independent RNA-seq data in mock and *Pso* treatments are presented where DEGs were selected at *P* adjusted value < 0.01.

Figure S7 Features of differentially expressed genes (DEGs) in *Pseudomonas syringae* pv. *oryzae* (*Pso*)-treated 9-WT and *hac701* transcriptomes. Overlap and GO-analysis of upregulated (*A*) and downregulated (*B*) genes in *hac701* under *Pso* treatment. Transcriptome data were normalized using mock data sets for each genotype. GO enrichment analysis showing only the "Biological Process" of upregulated *HAC701*-repressed genes (141) and HAC701-dependent genes (336), downregulated *HAC701*-enhanced genes (31) and HAC701-dependent genes (46). Fold Enrichment Value uses Fisher's Exact test with results for uncorrected $P<0.05$.

Figure S8 Alignment of KIX domain found in different organisms. KIX domain in HAC701 (*A*) and HAC703 (*B*) proteins. Sc: *Saccharomyces cerevisiae*, Os: *Oryza sativa*, Hs: *Homo sapiens*, Ce: *Caenorhabditis elegans*, Dm: *Drosophila melanogaster*, Mm: *Mus musculus*.

Figure S9 *OsWRKY45* promoter contains a rare CRE motif. (*A*) CRE motif cluster found in 1kb upstream sequences of *OsWRKY45* start site. The red line indicates the probability of transcription factors binding to these CRE motif sites. CRE motif is found most probably on the direct strand (+). (*B*) 5 genes out of 660 DEGs (0.76%) in the *hac701* contain the CRE motif. Cister parameter settings: default settings were used.

Figure S10 Enrichment strength of ChIP signals in 9-WT input and histone modifications.

Figure S11 Heatmaps of genome-wide histone modification enrichments in genes and transposable elements (TEs) of rice 9-WT and *hac701* (*9-12b*$^{-/-}$) mutant. Enrichment of H3K9 acetylation, H3K9 di-methylation, H3K9 tri-methylation, H3K27 acetylation, and H3 in genes (*A*) and TE (*B*) regions. Data represent one of the two biologically independent samples showing similar enrichment results.

Figure S12 Heatmaps of genome-wide histone modification enrichments in simple repeats of rice 9-WT and *hac701* (*9-12b*$^{-/-}$) mutant. Enrichment of H3K9 acetylation, H3K9 di-methylation, H3K9 tri-methylation, H3K27 acetylation, and H3 in simple repeat regions. Data represent one of the two biologically independent samples showing similar enrichment results.

Figure S13 Enrichment scores of additional representative genes showing differential enrichments of H3K9 acetylation in *hac701* (*9-12b*$^{-/-}$) mutant. (*A*) Transcriptional coactivator genes showing reduced or partially reduced H3K9 acetylation enrichments. (*B*) Putative guard genes showing differential enrichments of H3K9 acetylation. Scores are averages of two biologically independent samples with bars showing standard deviation (SD).

Figure S14 Distribution on genomic locations of 265 regions in H3K9 acetylation ChIP (wild type/mutant).

Figure S15 *OsWRKY45* depth graph of H3K9 and H3K27 acetylation ChIP-seq showing the number of reads in RPKM (Reads Per Kilobase of transcript, per Million mapped reads) in 9-WT and *hac701* (*9-12b*$^{-/-}$) mutant. The red dotted box shows the 1 kb upstream region of *OsWRKY45* with arrow indicating the direction of transcription. Data show a representative sample.

Figure S16 *OsWRKY45* depth graph of H3K9 acetylation and H3K9 di-methylation ChIP-seq showing the number of reads in RPKM (Reads Per Kilobase of transcript, per Million mapped reads) in 9-WT and *hac701* (*9-12b*$^{-/-}$) mutant. The red dotted box shows the 1 kb upstream region of *OsWRKY45* with arrow indicating the direction of transcription. Data show a representative sample.

Figure S17 *OsWRKY45* depth graph of H3K9 acetylation and H3K9 tri-methylation ChIP-seq showing the number of reads in RPKM (Reads Per Kilobase of transcript, per Million mapped reads) in 9-WT and *hac701* (*9-12b*$^{-/-}$) mutant. The red dotted box shows the 1 kb

upstream region of *OsWRKY45* with arrow indicating the direction of transcription. Data show a representative sample.

Figure S18 Systemic gene expression analysis in rice-*Pseudomonas syringae* pv. *oryzae* (*Pso*) pathosystem. (*A*) Differentially expressed genes (DEGs) in the local (870) and systemic (24) tissues of plants infected with *Pso*. Eight DEGs were found to be common in both local and systemic tissues. (*B*) The expression of eight DEGs shown in log2 fold changes. For local tissue analysis, two independent RNA-seq samples in both treatments (mock and *Pso*) are presented. For systemic tissue analysis, two independent RNA-seq samples in mock and three in *Pso* treatment are presented. The number of reads are in RPKM (Reads Per Kilobase of transcript, per Million mapped reads) in 9-WT and *hac701*.

Figure S19 MA-plot of differentially expressed genes (DEGs) in systemic tissues of 9-WT and *hac701* infected with *Pseudomonas syringae* pv. *oryzae* (*Pso*). (*A*) and (*B*) plots showing differences in measurements of differentially expressed genes (DEGs). *P* adjusted value is set at <0.01. For 9-WT and *hac701* samples, two independent RNA-seq samples in mock treatment and three in *Pso* treatment are presented.

Figure S20 *OsWRKY45*-dependent defense pathway is suppressed by *HAC701*. Defense-related genes regulated directly and indirectly by *OsWRKY45* are negatively regulated by *HAC701* resulting in resistance phenotype of *hac701* through *OsWRKY45* upregulation.

SUPPLEMENTARY TABLE LEGENDS

Table S1 sgRNA oligonucleotides used for CRISPR/Cas9 mutagenesis and primers for genotyping. Bold sequences in the guide RNAs are the Protospacer Adjacent Motif (PAM).

Table S2 Summary of total RNA-sequencing data in local tissues.

Table S3 *HAC701* repressed and enhanced genes.

Table S4 Wild type (9-WT) DEGs in *Pso*.

Table S5 *HAC701* mutation DEGs in *Pso* (*HAC701mut*-DEGs in *Pso*). The motifs were identified 1kb upstream sequence of the start codon.

Table S6 *HAC701* mutation DEGs in Mock (*HAC701mut*-DEGs in Mock).

Table S7 BTH-responsive genes (24 hpi) in microarray experiments (34, 81) (Shimono et al. 2007, The Plant Cell & Sugano et al. 2010, Plant Molecular Biology). Overlap genes were removed.

Table S8 BTH-inducible & WRKY45-dependent genes (33) (Nakayama et al. 2013, BMC Plant Biology).

Table S9 Upregulated genes after DEX-induced *WRKY45* expression (33) (Nakayama et al. 2013, BMC Plant Biology).

Table S10 BTH-inducible genes affected by rice *NPR1* knockdown (81) (Sugano et al. 2010, Plant Molecular Biology).

Table S11 *HAC701* mutation DEGs found in BTH-WRKY45 regulated genes that contain W-box motifs. The motifs were identified 1 kb upstream sequence of the start codon.

Table S12 *HAC701* mutation DEGs found in BTH-WRKY45 and BTH-NPR1 regulated genes that contain W-box motifs. The motifs were identified 1 kb upstream sequence of the start codon.

Table S13 Rice ChIP-sequencing information of histone modifications.

Table S14 Identified peaks in H3K9ac and their corresponding genes in 9-WT/*9-12b*$^{-/-}$ (wild type/mutant). Colored boxes indicate the repeated genes.

Table S15 Identified peaks in H3K9me3 and their corresponding genes in *9-12b*$^{-/-}$/Input (mutant/Input). Colored boxes indicate repeated genes.

Table S16 Summary of total RNA-sequencing data in systemic tissues.

Table S17 List of R genes upregulated in *hac701* in *Pso*.

Table S18 Oligonucleotides used for RT-qPCRs (1) and ChIP-qPCRs (2).

ACKNOWLEDGEMENTS

We thank OIST SQC for RNA-seq and ChIP-seq analysis. This project benefited greatly from the comments of Drs. Yusuke Saijo, Hirofumi Nakagami, Justin Walley, and from the members of the Plant Epigenetics Unit (OIST) and Plant Immunity Research Group (RIKEN CSRS).

FUNDING

This work was supported in part by the Okinawa Institute of Science and Technology Graduate University (OIST). N.A.E. was also funded by Grant-in-Aid for JSPS Fellows (Grant No: 18F18085). The funders had no role in study design, data collection and analysis, decision to publish, or preparation of the manuscript.

AUTHOR CONTRIBUTIONS

NAE: Conceptualization, Data curation, Funding acquisition, Formal analysis, Investigation, Visualization, Writing-original draft, Writing-review & editing

LNT: Data curation, Formal analysis, Writing-review & editing

SM: Formal analysis, Investigation

YS: Formal analysis, Investigation

KS: Funding acquisition, Formal analysis, Supervision, Writing-review & editing

HS: Funding acquisition, Formal analysis, Investigation, Supervision, Writing-review & editing

COMPETING INTERESTS

The authors have declared that no competing interests exist.

REFERENCES

1. Lee KK & Workman JL (2007) Histone acetyltransferase complexes: one size doesn't fit all. *Nat. Rev. Mol. Cell Biol.* 8(4):284-295.

2. Chan HM & La Thangue NB (2001) p300/CBP proteins: HATs for transcriptional bridges and scaffolds. *J. Cell Sci.* 114(Pt 13):2363-2373.

3. Kalkhoven E (2004) CBP and p300: HATs for different occasions. *Biochem. Pharmacol.* 68(6):1145-1155.

4. Janknecht R & Hunter T (1996) Transcription. A growing coactivator network. *Nature* 383(6595):22-23.

5. Goodrich JA & Tjian R (1994) TBP-TAF complexes: selectivity factors for eukaryotic transcription. *Curr. Opin. Cell Biol.* 6(3):403-409.

6. Pandey R, *et al.* (2002) Analysis of histone acetyltransferase and histone deacetylase families of Arabidopsis thaliana suggests functional diversification of chromatin modification among multicellular eukaryotes. *Nucleic Acids Res.* 30(23):5036-5055.

7. Liu X, *et al.* (2012) Histone acetyltransferases in rice (Oryza sativa L.): phylogenetic analysis, subcellular localization and expression. *BMC Plant Biol.* 12:145.

8. Fang H, Liu X, Thorn G, Duan J, & Tian L (2014) Expression analysis of histone acetyltransferases in rice under drought stress. *Biochem. Biophys. Res. Commun.* 443(2):400-405.

9. Ma X, Lv S, Zhang C, & Yang C (2013) Histone deacetylases and their functions in plants. *Plant Cell Rep.* 32(4):465-478.

10. Song G & Walley JW (2016) Dynamic Protein Acetylation in Plant–Pathogen Interactions. *Frontiers in plant science* 7.

11. Ding B & Wang GL (2015) Chromatin versus pathogens: the function of epigenetics in plant immunity. *Frontiers in plant science* 6:675.

12. Zhu QH, Shan WX, Ayliffe MA, & Wang MB (2016) Epigenetic Mechanisms: An Emerging Player in Plant-Microbe Interactions. *Molecular plant-microbe interactions : MPMI* 29(3):187-196.

13. Fu W, Wu K, & Duan J (2007) Sequence and expression analysis of histone deacetylases in rice. *Biochem. Biophys. Res. Commun.* 356(4):843-850.

14. Yuan LW & Giordano A (2002) Acetyltransferase machinery conserved in p300/CBP-family proteins. *Oncogene* 21(14):2253-2260.

15. Ogryzko VV, Schiltz RL, Russanova V, Howard BH, & Nakatani Y (1996) The transcriptional coactivators p300 and CBP are histone acetyltransferases. *Cell* 87(5):953-959.

16. Bannister AJ & Kouzarides T (1996) The CBP co-activator is a histone acetyltransferase. *Nature* 384(6610):641-643.

17. Henry RA, Kuo YM, & Andrews AJ (2013) Differences in specificity and selectivity between CBP and p300 acetylation of histone H3 and H3/H4. *Biochemistry* 52(34):5746-5759.

18. Jin Q, *et al.* (2011) Distinct roles of GCN5/PCAF-mediated H3K9ac and CBP/p300-mediated H3K18/27ac in nuclear receptor transactivation. *EMBO J.* 30(2):249-262.

19. Tie F, *et al.* (2009) CBP-mediated acetylation of histone H3 lysine 27 antagonizes Drosophila Polycomb silencing. *Development* 136(18):3131-3141.

20. Das C, Lucia MS, Hansen KC, & Tyler JK (2009) CBP/p300-mediated acetylation of histone H3 on lysine 56. *Nature* 459(7243):113-117.

21. Schiltz RL, *et al.* (1999) Overlapping but distinct patterns of histone acetylation by the human coactivators p300 and PCAF within nucleosomal substrates. *J. Biol. Chem.* 274(3):1189-1192.

22. Sakamoto S, *et al.* (2012) E2A and CBP/p300 act in synergy to promote chromatin accessibility of the immunoglobulin kappa locus. *J. Immunol.* 188(11):5547-5560.

23. Modak R, *et al.* (2013) Probing p300/CBP associated factor (PCAF)-dependent pathways with a small molecule inhibitor. *ACS chemical biology* 8(6):1311-1323.

24. Espinas NA, Saze H, & Saijo Y (2016) Epigenetic Control of Defense Signaling and Priming in Plants. *Frontiers in plant science* 7.

25. Kuwata H (1985) Pseudomonas syringiae pv. oryzae pv. nov., causal agent of bacterial halo blight of rice. *Ann Phytopath. Soc. Japan* 51:212-218.

26. Kang S, Kang K, Lee K, & Back K (2007) Characterization of rice tryptophan decarboxylases and their direct involvement in serotonin biosynthesis in transgenic rice. *Planta* 227(1):263-272.

27. Ishihara A, *et al.* (2008) The tryptophan pathway is involved in the defense responses of rice against pathogenic infection via serotonin production. *Plant J.* 54(3):481-495.

28. Shimizu T, *et al.* (2012) Purification and identification of naringenin 7-O-methyltransferase, a key enzyme in biosynthesis of flavonoid phytoalexin sakuranetin in rice. *J. Biol. Chem.* 287(23):19315-19325.

29. Ogawa S, *et al.* (2017) OsMYC2, an essential factor for JA-inductive sakuranetin production in rice, interacts with MYC2-like proteins that enhance its transactivation ability. *Scientific reports* 7:40175.

30. Swaminathan S, Morrone D, Wang Q, Fulton DB, & Peters RJ (2009) CYP76M7 is an ent-cassadiene C11alpha-hydroxylase defining a second multifunctional diterpenoid biosynthetic gene cluster in rice. *Plant Cell* 21(10):3315-3325.

31. Vanholme R, Demedts B, Morreel K, Ralph J, & Boerjan W (2010) Lignin biosynthesis and structure. *Plant Physiol.* 153(3):895-905.

32. Wang Q, *et al.* (2012) Characterization of CYP76M5-8 indicates metabolic plasticity within a plant biosynthetic gene cluster. *J. Biol. Chem.* 287(9):6159-6168.

33. Nakayama A, *et al.* (2013) Genome-wide identification of WRKY45-regulated genes that mediate benzothiadiazole-induced defense responses in rice. *BMC Plant Biol.* 13(150).

34. Shimono M, *et al.* (2007) Rice WRKY45 plays a crucial role in benzothiadiazole-inducible blast resistance. *Plant Cell* 19(6):2064-2076.

35. Cheng X, *et al.* (2019) Structural basis of dimerization and dual W-box DNA recognition by rice WRKY domain. *Nucleic Acids Res.* 47(8):4308-4318.

36. Parker D, *et al.* (1996) Phosphorylation of CREB at Ser-133 induces complex formation with CREB-binding protein via a direct mechanism.pdf>. *Mol. Cell. Biol.*:694-703.

37. Yadav A, Thakur JK, & Yadav G (2017) KIXBASE: A comprehensive web resource for identification and exploration of KIX domains. *Scientific reports* 7(1):14924.

38. Dancy BM & Cole PA (2015) Protein Lysine Acetylation by p300/CBP. *Chemical reviews* 115(6):2419-2452.

39. Du Z, *et al.* (2013) Genome-wide analysis of histone modifications: H3K4me2, H3K4me3, H3K9ac, and H3K27ac in Oryza sativa L. Japonica. *Molecular plant* 6(5):1463-1472.

40. Sarris PF, Cevik V, Dagdas G, Jones JD, & Krasileva KV (2016) Comparative analysis of plant immune receptor architectures uncovers host proteins likely targeted by pathogens. *BMC Biol.* 14:8.

41. Weidenbach D, *et al.* (2016) Polarized Defense Against Fungal Pathogens Is Mediated by the Jacalin-Related Lectin Domain of Modular Poaceae-Specific Proteins. *Molecular plant* 9(4):514-527.

42. Singh P, *et al.* (2014) Environmental History Modulates Arabidopsis Pattern-Triggered Immunity in a HISTONE ACETYLTRANSFERASE1-Dependent Manner. *Plant Cell*.

43. Kim S, *et al.* (2020) GCN5 modulates salicylic acid homeostasis by regulating H3K14ac levels at the 5' and 3' ends of its target genes. *Nucleic Acids Res*. 48(11):5953-5966.

44. De Vleesschauwer D, Gheysen G, & Hofte M (2013) Hormone defense networking in rice: tales from a different world. *Trends Plant Sci.* 18(10):555-565.

45. Vidhyasekaran P (2016) *Switching on plant innate immunity signaling systems* (Springer International Publishing, Switzerland).

46. De Vleesschauwer D, Xu J, & Hofte M (2014) Making sense of hormone-mediated defense networking: from rice to Arabidopsis. *Frontiers in plant science* 5:611.

47. Yang DL, Yang Y, & He Z (2013) Roles of plant hormones and their interplay in rice immunity. *Molecular plant* 6(3):675-685.

48. Yan S & Dong X (2014) Perception of the plant immune signal salicylic acid. *Curr. Opin. Plant Biol.* 20:64-68.

49. Silverman P, *et al.* (1995) Salicylic acid in rice (biosynthesis, conjugation, and possible role). *Plant Physiol.* 108:633-639.

50. Chen Z, Iyer S, Caplan A, Klessig DF, & Fan B (1997) Differential accumulation of salicylic acid and salicylic acid-sensitive catalase in different rice tissues. *Plant Physiol.* 114:193-201.

51. Hiebert CW, *et al.* (2020) Stem rust resistance in wheat is suppressed by a subunit of the mediator complex. *Nature communications* 11(1):1123.

52. Brownell JE & Allis CD (1996) Special HATs for special occasions: linking histone acetylation to chromatin assembly and gene activation. *Curr. Opin. Genet. Dev.* 6:176-184.

53. Poss ZC, Ebmeier CC, & Taatjes DJ (2013) The Mediator complex and transcription regulation. *Crit. Rev. Biochem. Mol. Biol.* 48(6):575-608.

54. Canet JV, Dobon A, & Tornero P (2012) Non-recognition-of-BTH4, an Arabidopsis mediator subunit homolog, is necessary for development and response to salicylic acid. *Plant Cell* 24(10):4220-4235.

55. van der Hoorn RA & Kamoun S (2008) From Guard to Decoy: a new model for perception of plant pathogen effectors. *Plant Cell* 20(8):2009-2017.

56. Jackson JP, *et al.* (2004) Dimethylation of histone H3 lysine 9 is a critical mark for DNA methylation and gene silencing in Arabidopsis thaliana. *Chromosoma* 112(6):308-315.

57. Karasov T, Chae E, Herman J, & Bergelson J (2017) Mechanisms to Mitigate the Tradeoff between Growth and Defense. *Plant Cell*.

58. Huot B, Yao J, Montgomery BL, & He SY (2014) Growth-defense tradeoffs in plants: a balancing act to optimize fitness. *Molecular plant* 7(8):1267-1287.

59. Xie K & Yang Y (2013) RNA-guided genome editing in plants using a CRISPR-Cas system. *Molecular plant* 6(6):1975-1983.

60. Heese A, *et al.* (2007) The receptor-like kinase SERK3/BAK1 is a central regulator of innate immunity in plants. *Proceedings of the National Academy of Sciences of the United States of America* 104(29):12217-12222.

61. Park CJ & Ronald PC (2012) Cleavage and nuclear localization of the rice XA21 immune receptor. *Nature communications* 3:920.

62. Liu X, *et al.* (2015) Bacterial Leaf Infiltration Assay for Fine Characterization of Plant Defense Responses using the Arabidopsis thaliana-Pseudomonas syringae Pathosystem. *J Vis Exp* (104).

63. Pfaffl MW (2001) A new mathematical model for relative quantification in real-time RT-PCR. *Nucleic Acids Res.* 29(9):e45.

64. Saleh A, Alvarez-Venegas R, & Avramova Z (2008) An efficient chromatin immunoprecipitation (ChIP) protocol for studying histone modifications in Arabidopsis plants. *Nature protocols* 3(6):1018-1025.

65. Trapnell C, Pachter L, & Salzberg SL (2009) TopHat: discovering splice junctions with RNA-Seq. *Bioinformatics* 25(9):1105-1111.

66. Trapnell C, *et al.* (2012) Differential gene and transcript expression analysis of RNA-seq experiments with TopHat and Cufflinks. *Nature protocols* 7(3):562-578.

67. Love MI, Huber W, & Anders S (2014) Moderated estimation of fold change and dispersion for RNA-seq data with DESeq2. *Genome biology* 15(12):550.

68. Li Q, Brown JB, Huang H, & Bickel PJ (2011) Measuring reproducibility of high-throughput experiments. *The Annals of Applied Statistics* 5(3):1752-1779.

69. Consortium TGO (2017) Expansion of the Gene Ontology knowledgebase and resources. *Nucleic Acids Res.* 45(D1):D331-D338.

70. Consortium TGO (2000) Gene Ontology: tool for the unification of biology. *Nat. Genet.* 25:25-29.

71. Consortium TGO (2015) Gene Ontology Consortium: going forward. *Nucleic Acids Res.* 43(Database issue):D1049-1056.

72. Heberle H, Meirelles GV, da Silva FR, Telles GP, & Minghim R (2015) InteractiVenn: a web-based tool for the analysis of sets through Venn diagrams. *BMC Bioinformatics* 16:169.

73. Langmead B, Trapnell C, Pop M, & Salzberg SL (2009) Ultrafast and memory-efficient alignment of short DNA sequences to the human genome. *Genome biology* 10(3):R25.

74. Freese NH, Norris DC, & Loraine AE (2016) Integrated genome browser: visual analytics platform for genomics. *Bioinformatics* 32(14):2089-2095.

75. Ramirez F, *et al.* (2016) deepTools2: a next generation web server for deep-sequencing data analysis. *Nucleic Acids Res*. 44(W1):W160-165.

76. Quinlan AR & Hall IM (2010) BEDTools: a flexible suite of utilities for comparing genomic features. *Bioinformatics* 26(6):841-842.

77. Heinz S, *et al.* (2010) Simple combinations of lineage-determining transcription factors prime cis-regulatory elements required for macrophage and B cell identities. *Mol. Cell* 38(4):576-589.

78. Dereeper A, *et al.* (2008) Phylogeny.fr: robust phylogenetic analysis for the non-specialist. *Nucleic Acids Res.* 36(Web Server issue):W465-469.

79. Edgar RC (2004) MUSCLE: multiple sequence alignment with high accuracy and high throughput. *Nucleic Acids Res.* 32(5):1792-1797.

80. Frith M, Hansen U, & Weng Z (2001) Detection of cis-element clusters in higher eukaryotic DNA. *Bioinformatics* 17:878-889.

81. Sugano S, *et al.* (2010) Role of OsNPR1 in rice defense program as revealed by genome-wide expression analysis. *Plant Mol. Biol.* 74(6):549-562.

Figure 1

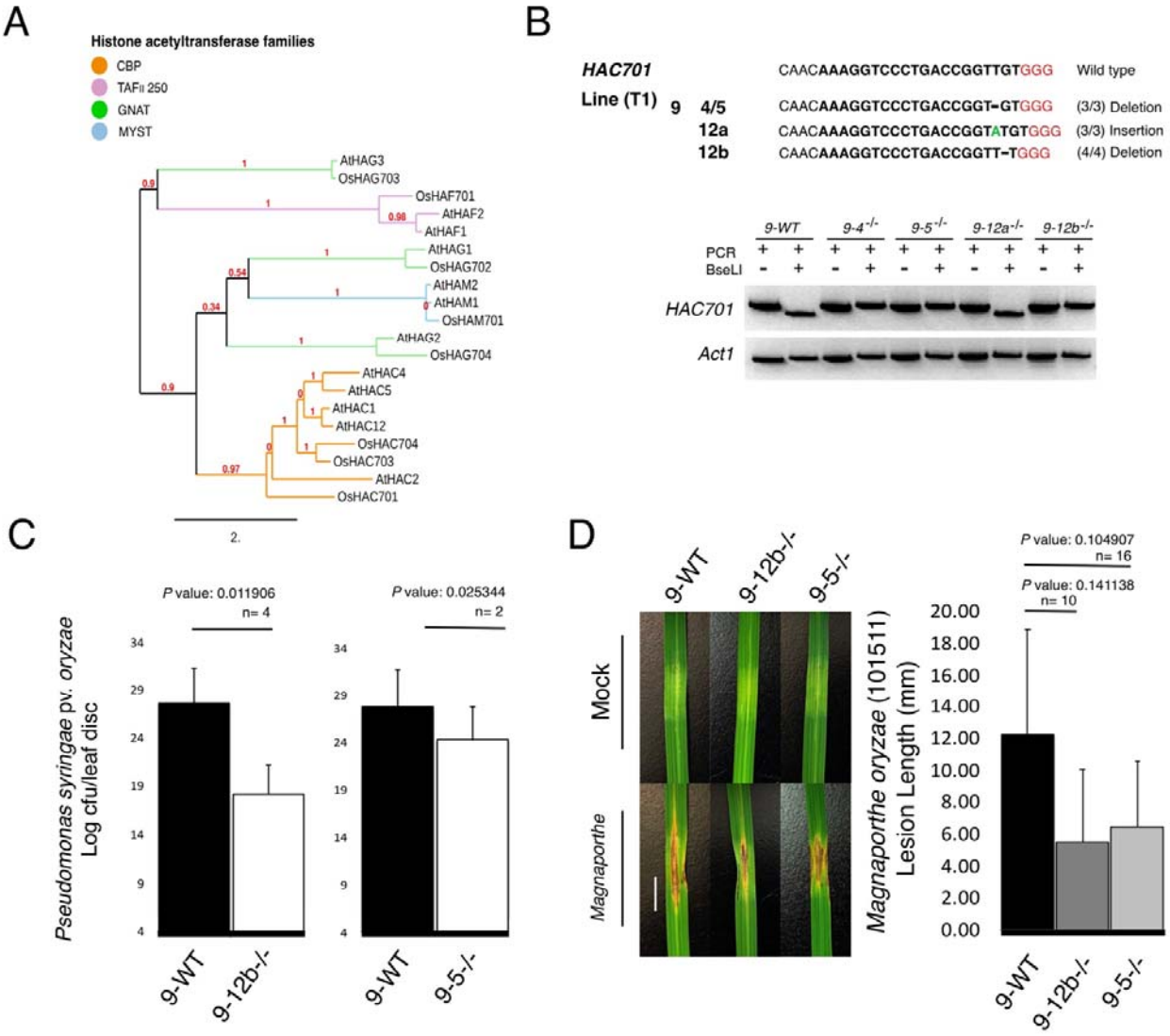
A
Histone acetyltransferase families
CBP
TAFII 250
GNAT
MYST
AtHAG3
OsHAG703
OsHAF701
AtHAF2
AtHAF1
AtHAG1
OsHAG702
AtHAM2
AtHAM1
OsHAM701
AtHAG2
OsHAG704
AtHAC4
AtHAC5
AtHAC1
AtHAC12
OsHAC704
OsHAC703
AtHAC2
OsHAC701
2.
B
HAC701
Line (T1)
9
4/5
12a
12b
CAACAAAGGTCCCTGACCGGTTGTGGG Wild type
CAACAAAGGTCCCTGACCGGT-GTGGG (3/3) Deletion
CAACAAAGGTCCCTGACCGGTATGTGGG (3/3) Insertion
CAACAAAGGTCCCTGACCGGTT-TGGG (4/4) Deletion
9-WT
9-4-/-
9-5-/-
9-12a-/-
9-12b-/-
PCR
BseLI
HAC701
Act1
C
Pseudomonas syringae pv. oryzae
Log cfu/leaf disc
P value: 0.011906
n= 4
P value: 0.025344
n= 2
9-WT
9-12b-/-
9-5-/-
D
9-WT
9-12b-/-
9-5-/-
Mock
Magnaporthe
Magnaporthe oryzae (101511)
Lesion Length (mm)
P value: 0.104907
n= 16
P value: 0.141138
n= 10
9-WT
9-12b-/-
9-5-/-

Figure 2

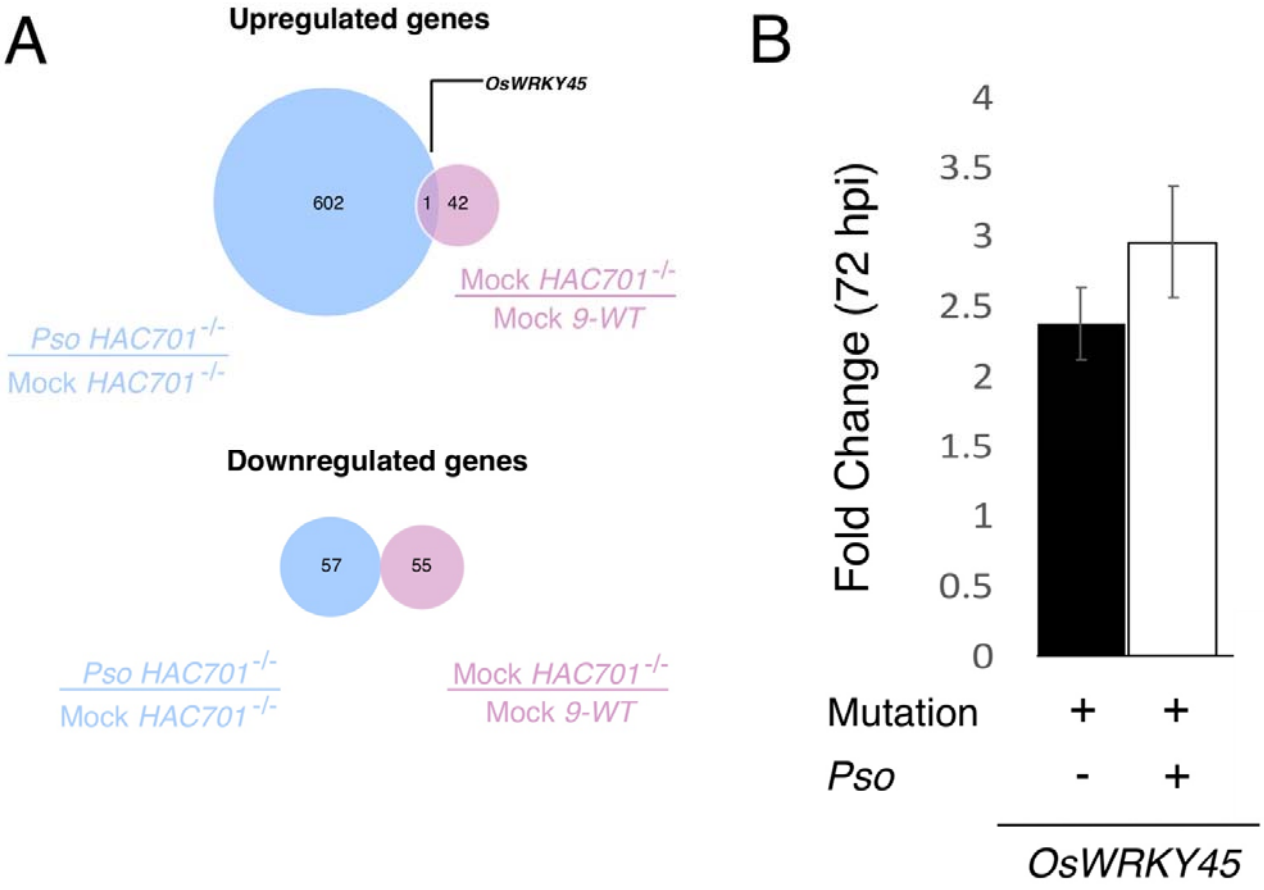
A
Upregulated genes
OsWRKY45
602
1
42
Mock HAC701-/-
Mock 9-WT
Pso HAC701-/-
Mock HAC701-/-
Downregulated genes
57
55
Pso HAC701-/-
Mock HAC701-/-
Mock HAC701-/-
Mock 9-WT
B
Fold Change (72 hpi)
4
3.5
3
2.5
2
1.5
1
0.5
0
Mutation + +
Pso - +
OsWRKY45

Figure 3

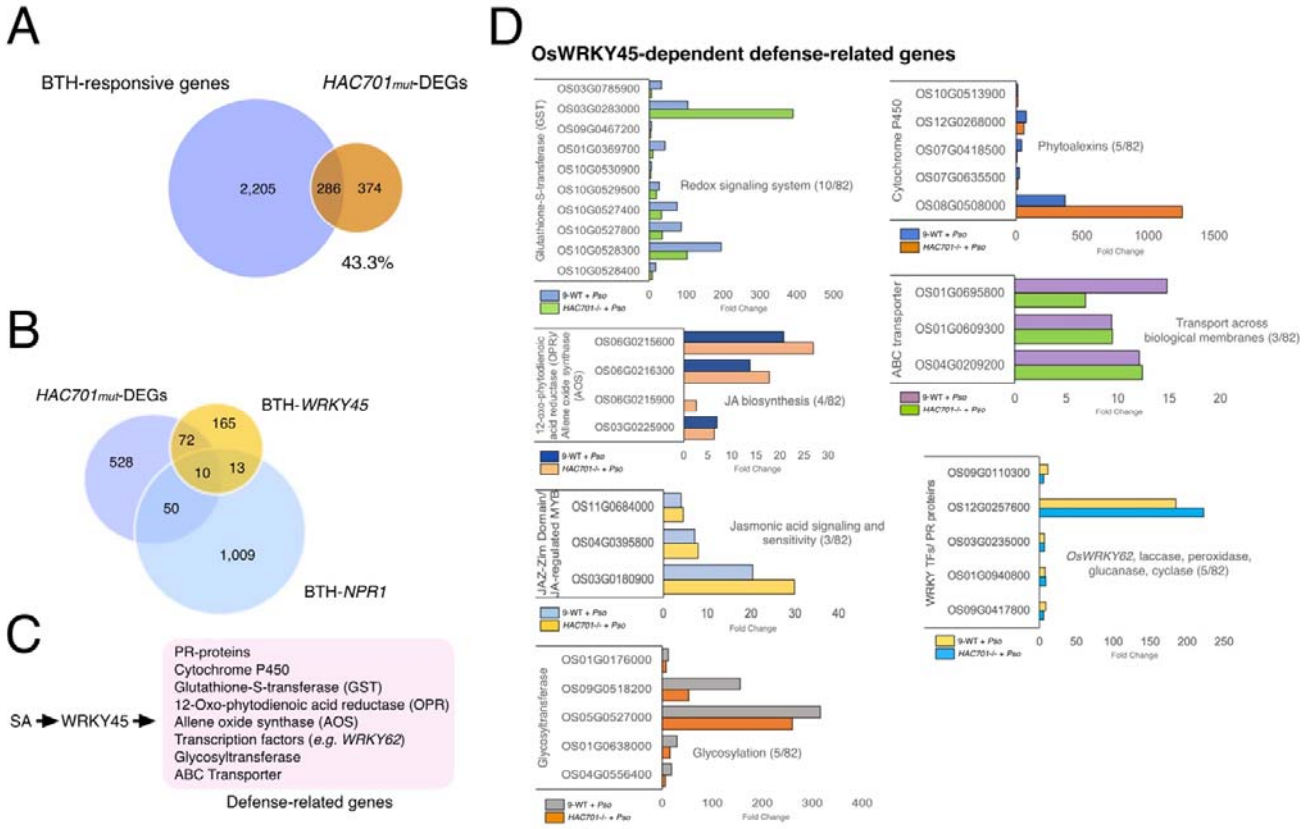
A
BTH-responsive genes
HAC701mut-DEGs
2,205
286
374
43.3%
B
HAC701mut-DEGs
BTH-WRKY45
BTH-NPR1
528
165
72
10
13
50
1,009
C
SA → WRKY45 →
PR-proteins
Cytochrome P450
Glutathione-S-transferase (GST)
12-Oxo-phytodienoic acid reductase (OPR)
Allene oxide synthase (AOS)
Transcription factors (e.g. WRKY62)
Glycosyltransferase
ABC Transporter
Defense-related genes
D
OsWRKY45-dependent defense-related genes
Glutathione-S-transferase (GST)
OS03G0785900
OS03G0283000
OS09G0467200
OS01G0369700
OS10G0530900
OS10G0529500
OS10G0527400
OS10G0527800
OS10G0528300
OS10G0528400
Redox signaling system (10/82)
Cytochrome P450
OS10G0513900
OS12G0268000
OS07G0418500
OS07G0635500
OS08G0508000
Phytoalexins (5/82)
ABC transporter
OS01G0695800
OS01G0609300
OS04G0209200
Transport across biological membranes (3/82)
12-oxo-phytodienoic acid reductase (OPR)/ Allene oxide synthase (AOS)
OS06G0215600
OS06G0216300
OS06G0215900
OS03G0225900
JA biosynthesis (4/82)
JAZ-Zim Domain/ JA-regulated MYB
OS11G0684000
OS04G0395800
OS03G0180900
Jasmonic acid signaling and sensitivity (3/82)
WRKY TFs/ PR proteins
OS09G0110300
OS12G0257600
OS03G0235000
OS01G0940800
OS09G0417800
OsWRKY62, laccase, peroxidase, glucanase, cyclase (5/82)
Glycosyltransferase
OS01G0176000
OS09G0518200
OS05G0527000
OS01G0638000
OS04G0556400
Glycosylation (5/82)
9-WT + Pso
HAC701-/- + Pso
Fold Change

Figure 4

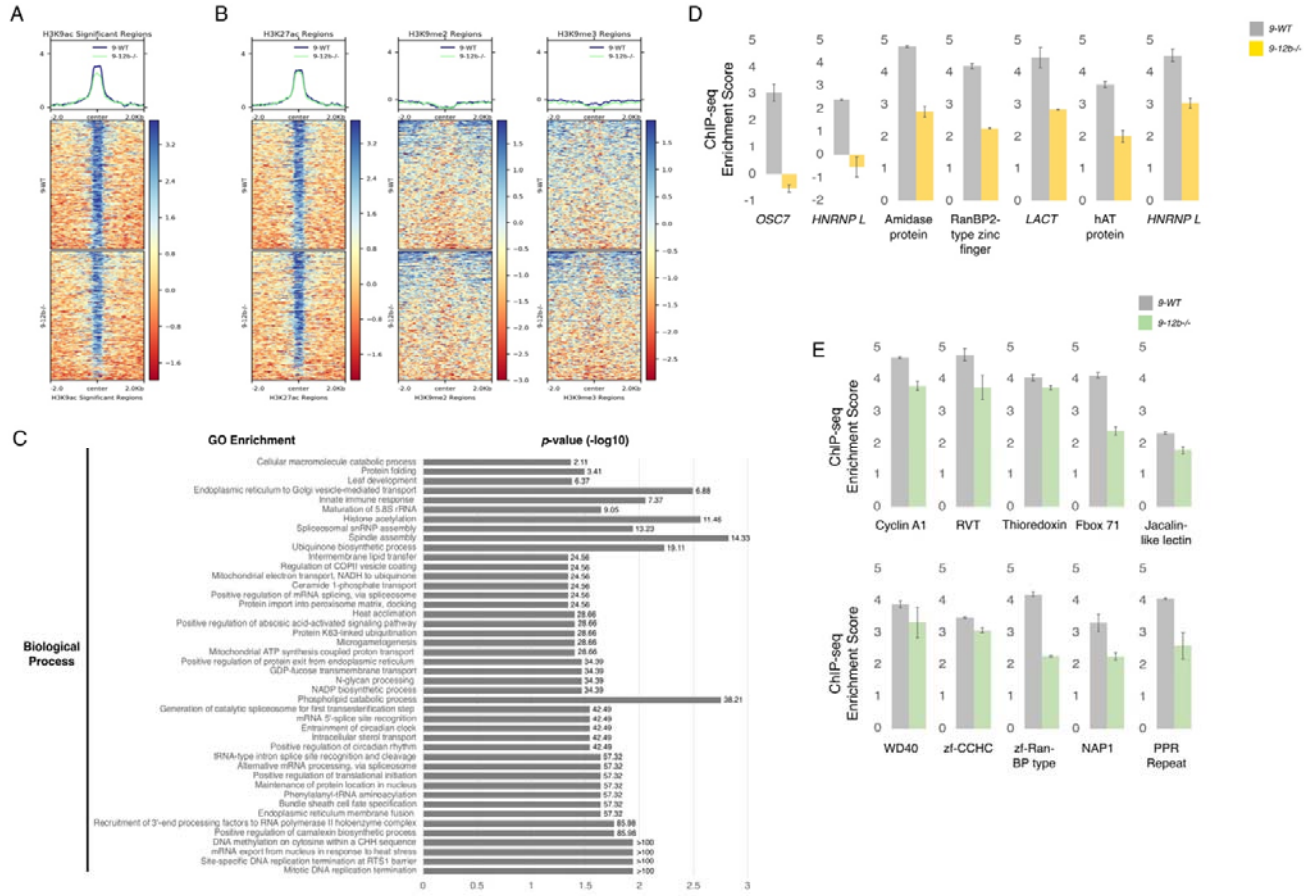
A
B
C
D
E
H3K9ac Significant Regions
H3K27ac Regions
H3K9me2 Regions
H3K9me3 Regions
9-WT
9-12b-/-
GO Enrichment
p-value (-log10)
Biological Process
Cellular macromolecule catabolic process
Protein folding
Leaf development
Endoplasmic reticulum to Golgi vesicle-mediated transport
Innate immune response
Maturation of 5.8S rRNA
Histone acetylation
Spliceosomal snRNP assembly
Spindle assembly
Ubiquinone biosynthetic process
Intermembrane lipid transfer
Regulation of COPII vesicle coating
Mitochondrial electron transport, NADH to ubiquinone
Ceramide 1-phosphate transport
Positive regulation of mRNA splicing, via spliceosome
Protein import into peroxisome matrix, docking
Heat acclimation
Positive regulation of abscisic acid-activated signaling pathway
Protein K63-linked ubiquitination
Microgametogenesis
Mitochondrial ATP synthesis coupled proton transport
Positive regulation of protein exit from endoplasmic reticulum
GDP-fucose transmembrane transport
N-glycan processing
NADP biosynthetic process
Phospholipid catabolic process
Generation of catalytic spliceosome for first transesterification step
mRNA 5'-splice site recognition
Entrainment of circadian clock
Intracellular sterol transport
Positive regulation of circadian rhythm
tRNA-type intron splice site recognition and cleavage
Alternative mRNA processing, via spliceosome
Positive regulation of translational initiation
Maintenance of protein location in nucleus
Phenylalanyl-tRNA aminoacylation
Bundle sheath cell fate specification
Endoplasmic reticulum membrane fusion
Recruitment of 3'-end processing factors to RNA polymerase II holoenzyme complex
Positive regulation of camalexin biosynthetic process
DNA methylation on cytosine within a CHH sequence
mRNA export from nucleus in response to heat stress
Site-specific DNA replication termination at RTS1 barrier
Mitotic DNA replication termination
ChIP-seq Enrichment Score
OSC7
HNRNP L
Amidase protein
RanBP2-type zinc finger
LACT
hAT protein
Cyclin A1
RVT
Thioredoxin
Fbox 71
Jacalin-like lectin
WD40
zf-CCHC
zf-Ran-BP type
NAP1
PPR Repeat

Figure 5

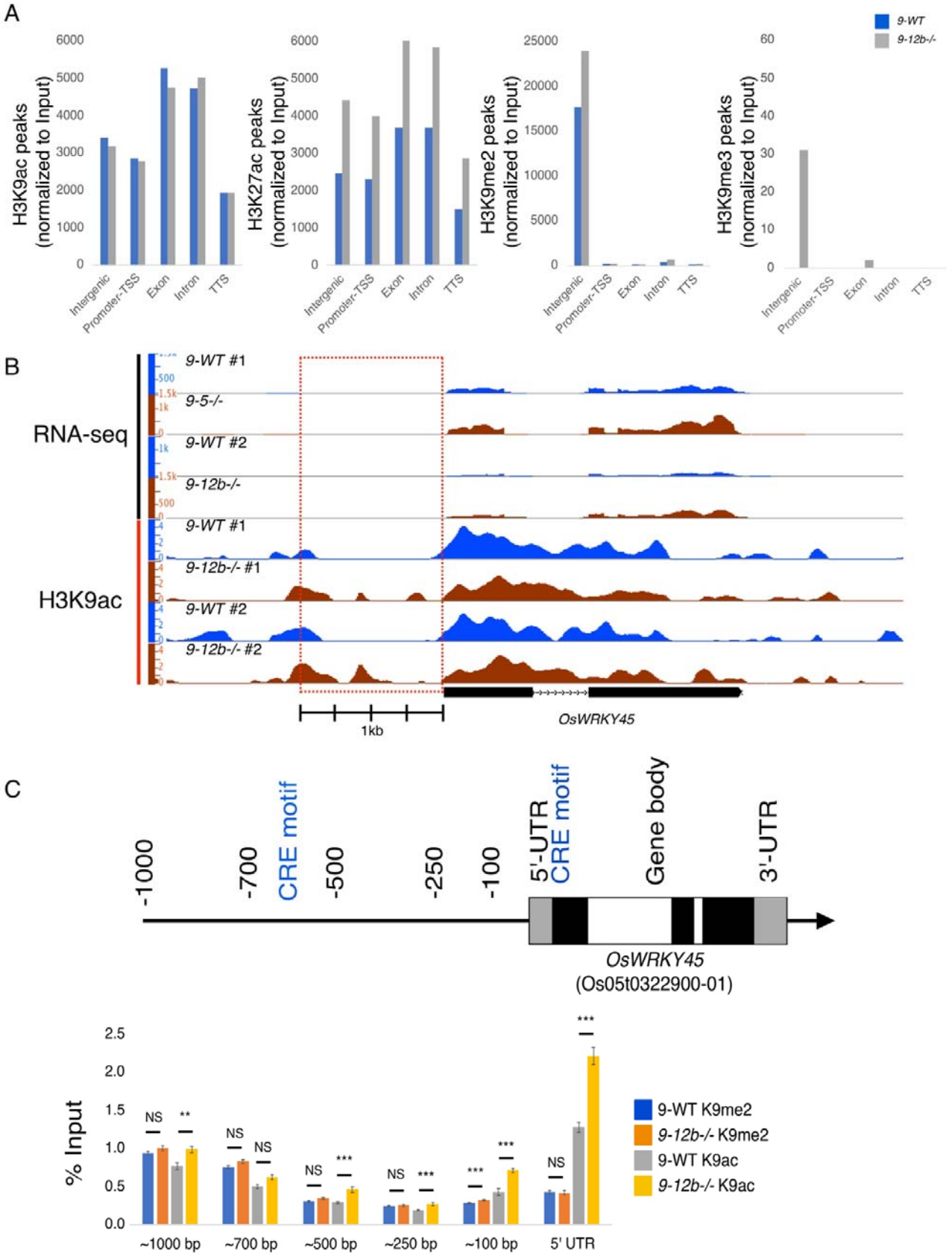
A
9-WT
9-12b-/-
H3K9ac peaks (normalized to Input)
H3K27ac peaks (normalized to Input)
H3K9me2 peaks (normalized to Input)
H3K9me3 peaks (normalized to Input)
Intergenic
Promoter-TSS
Exon
Intron
TTS
B
RNA-seq
H3K9ac
9-WT #1
9-5-/-
9-WT #2
9-12b-/-
9-12b-/- #1
9-12b-/- #2
1kb
OsWRKY45
C
-1000
-700
CRE motif
-500
-250
-100
5'-UTR
CRE motif
Gene body
3'-UTR
OsWRKY45
(Os05t0322900-01)
% Input
9-WT K9me2
9-12b-/- K9me2
9-WT K9ac
9-12b-/- K9ac
~1000 bp
~700 bp
~500 bp
~250 bp
~100 bp
5' UTR

Figure S1

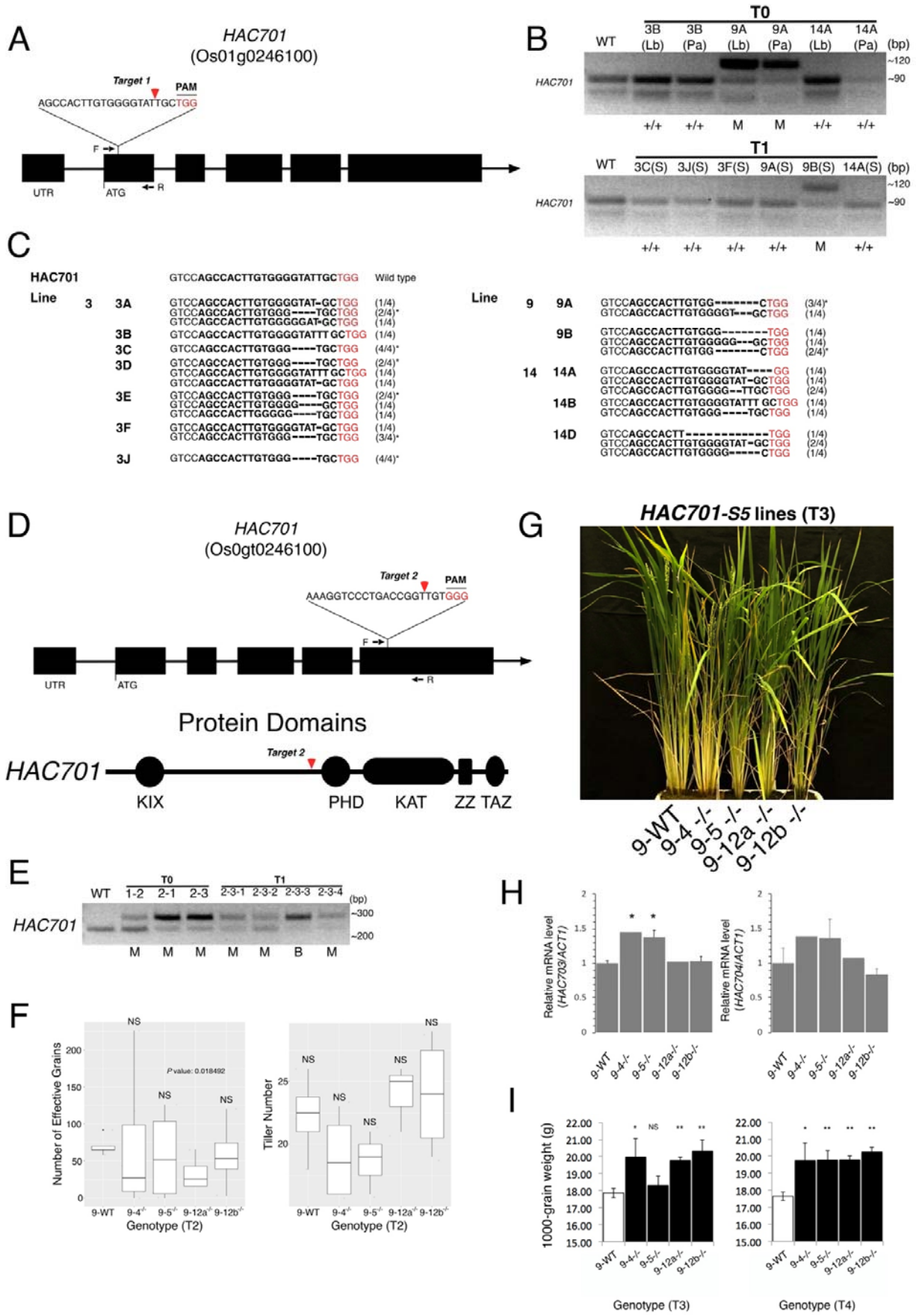
A
HAC701
(Os01g0246100)
Target 1
PAM
AGCCACTTGTGGGGTATTGCTGG
F
R
UTR
ATG
B
T0
WT
3B (Lb)
3B (Pa)
9A (Lb)
9A (Pa)
14A (Lb)
14A (Pa)
(bp)
~120
~90
HAC701
+/+ +/+ M M +/+ +/+
T1
WT
3C(S) 3J(S) 3F(S) 9A(S) 9B(S) 14A(S)
(bp)
~120
~90
HAC701
+/+ +/+ +/+ +/+ M +/+
C
HAC701 GTCCAGCCACTTGTGGGGTATTGCTGG Wild type
Line 3
3A GTCCAGCCACTTGTGGGGTAT-GCTGG (1/4)
GTCCAGCCACTTGTGGG----TGCTGG (2/4)*
GTCCAGCCACTTGTGGGGGAT-GCTGG (1/4)
3B GTCCAGCCACTTGTGGGGTATTT GCTGG (1/4)
3C GTCCAGCCACTTGTGGG----TGCTGG (4/4)*
3D GTCCAGCCACTTGTGGG----TGCTGG (2/4)*
GTCCAGCCACTTGTGGGGTATTT GCTGG (1/4)
GTCCAGCCACTTGTGGGGTAT-GCTGG (1/4)
3E GTCCAGCCACTTGTGGG----TGCTGG (2/4)*
GTCCAGCCACTTGTGGGG----GCTGG (1/4)
GTCCAGCCACTTGGGGG----TGCTGG (1/4)
3F GTCCAGCCACTTGTGGGGTAT-GCTGG (1/4)
GTCCAGCCACTTGTGGG----TGCTGG (3/4)*
3J GTCCAGCCACTTGTGGG----TGCTGG (4/4)*
Line 9
9A GTCCAGCCACTTGTGG-------CTGG (3/4)*
GTCCAGCCACTTGTGGGGT---GCTGG (1/4)
9B GTCCAGCCACTTGTGGG-------TGG (1/4)
GTCCAGCCACTTGTGGGGG---GCTGG (1/4)
GTCCAGCCACTTGTGG-------CTGG (2/4)*
14
14A GTCCAGCCACTTGTGGGGTAT----GG (1/4)
GTCCAGCCACTTGTGGGGTAT-GCTGG (1/4)
GTCCAGCCACTTGTGGGG--TTGCTGG (2/4)
14B GTCCAGCCACTTGTGGGGTATTT GCTGG (1/4)
GTCCAGCCACTTGTGGG----TGCTGG (1/4)
14D GTCCAGCCACTT----------TGG (1/4)
GTCCAGCCACTTGTGGGGTAT-GCTGG (2/4)
GTCCAGCCACTTGTGGGG-----CTGG (1/4)
D
HAC701
(Os0gt0246100)
Target 2
PAM
AAAGGTCCCTGACCGGTTGTGGG
F
R
UTR
ATG
Protein Domains
HAC701
Target 2
KIX
PHD
KAT
ZZ TAZ
G
HAC701-S5 lines (T3)
9-WT
9-4 -/-
9-5 -/-
9-12a -/-
9-12b -/-
E
T0
T1
WT 1-2 2-1 2-3 2-3-1 2-3-2 2-3-3 2-3-4
(bp)
~300
~200
HAC701
M M M M M B M
F
Number of Effective Grains
P value: 0.018492
NS
9-WT 9-4-/- 9-5-/- 9-12a-/- 9-12b-/-
Genotype (T2)
Tiller Number
NS
9-WT 9-4-/- 9-5-/- 9-12a-/- 9-12b-/-
Genotype (T2)
H
Relative mRNA level (HAC703/ACT1)
Relative mRNA level (HAC704/ACT1)
9-WT 9-4-/- 9-5-/- 9-12a-/- 9-12b-/-
I
1000-grain weight (g)
NS
9-WT 9-4-/- 9-5-/- 9-12a-/- 9-12b-/-
Genotype (T3)
Genotype (T4)

Figure S2

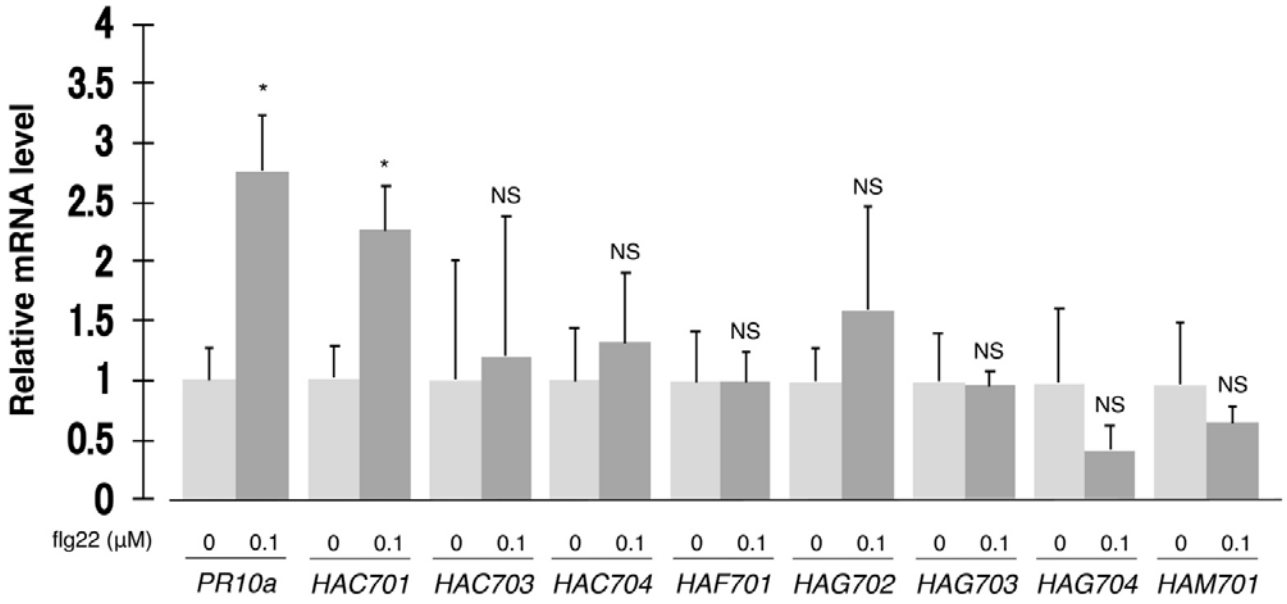
Relative mRNA level
4
3.5
3
2.5
2
1.5
1
0.5
0
*
*
NS
NS
NS
NS
NS
NS
NS
flg22 (μM)
0 0.1
PR10a
HAC701
HAC703
HAC704
HAF701
HAG702
HAG703
HAG704
HAM701

Figure S3

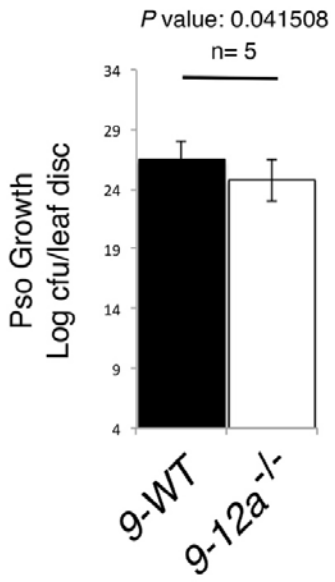
P value: 0.041508
n= 5
Pso Growth
Log cfu/leaf disc
34
29
24
19
14
9
4
9-WT
9-12a -/-

Figure S4

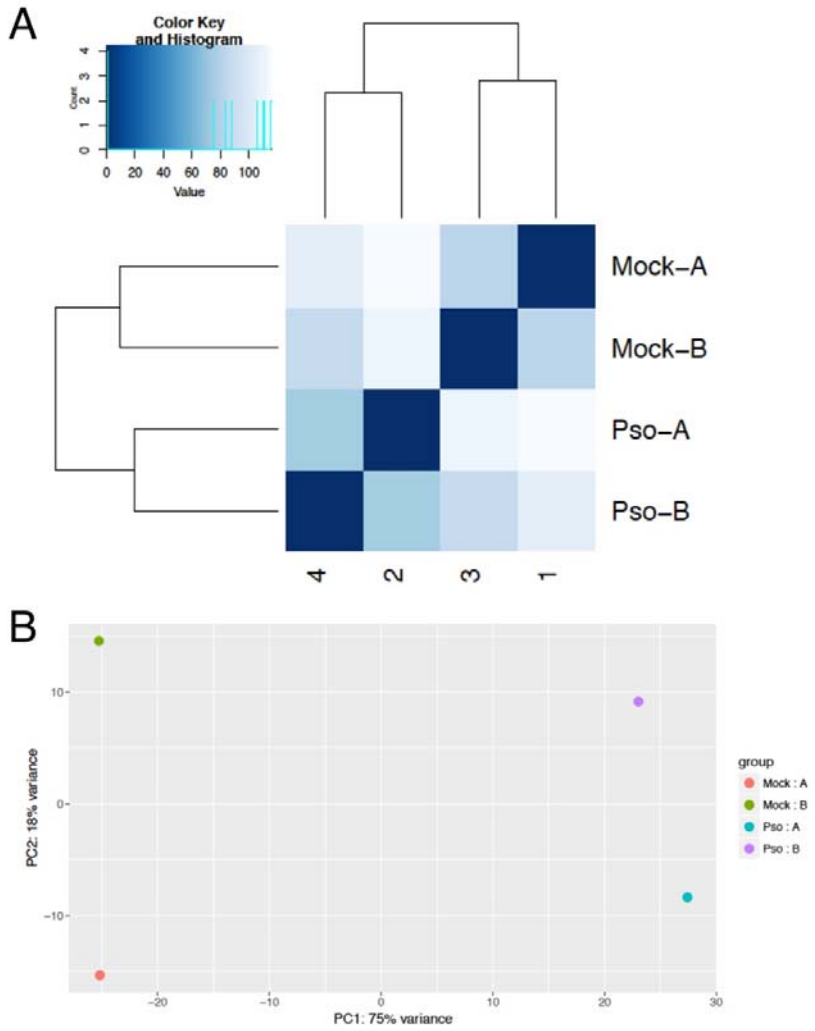
A
Color Key
and Histogram
Count
Value
Mock–A
Mock–B
Pso–A
Pso–B
4
2
3
1
B
PC2: 18% variance
PC1: 75% variance
group
Mock : A
Mock : B
Pso : A
Pso : B

Figure S5

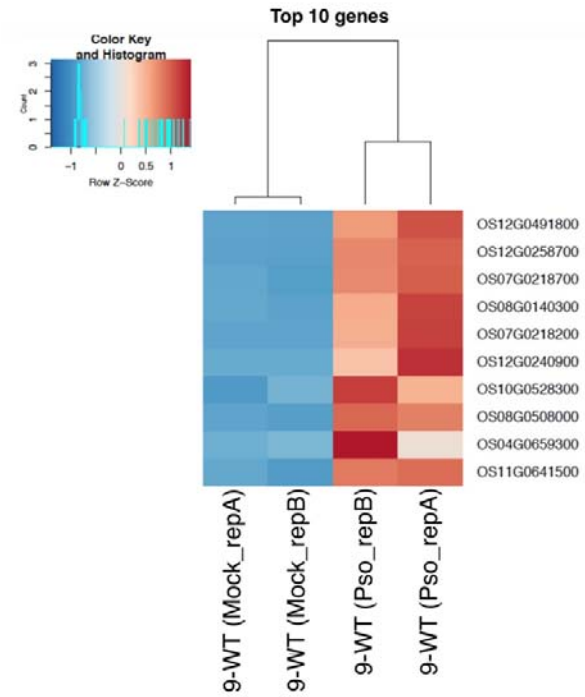

Gene ID	Description
OS12G0491800	Kaurene synthase-like 10
OS12G0258700	Laccase 29
OS07G0218700	Cytochrome P450 family protein
OS08G0140300	Tryptophan decarboxylase 1
OS07G0218200	Terpene synthase 3
OS12G0240900	Naringenin 7-O-methyltransferase
OS10G0528300	Tau glutathione S-transferase 4
OS08G0508000	Cytochrome P450 76M2
OS04G0659300	Root meander curling
OS11G0641500	Laccase 23

Figure S6

A

Highly enriched terms upon *Pseudomonas syringiae pv. oryzae* infection in 9-WT rice		
Up-regulated terms	Fold Enrichment	raw P-value
Cell wall macromolecule catabolic process	54.94	4.22E-07
Adventitious root development	54.94	3.54E-02
Lignin biosynthetic process	54.94	3.54E-02
Sphingolipid biosynthetic process	54.94	3.54E-02
Gibberellin biosynthetic process	54.94	3.54E-02
Chitin catabolic process	54.94	4.22E-07
Response to wounding	54.94	3.54E-02
Response to other organism	54.94	2.70E-08
ent-kaurene oxidation to kaurenoic acid	54.94	3.54E-02
Diterpene phytoalexin precursor biosynthetic process pathway	41.21	1.89E-04
Shikimate biosynthetic process	36.63	3.08E-03
Chorismate biosynthetic process	36.63	3.08E-03
Carbohydrate transport	18.31	8.32E-03
Carbohydrate metabolic process	5.78	6.62E-03
Electron transport chain	5.49	1.17E-03
Regulation of transcription, DNA templated	2.79	2.43E-02

Down-regulated terms	Fold Enrichment	raw P-value
Regulation of transcription, DNA templated	10.26	1.69E-02

B

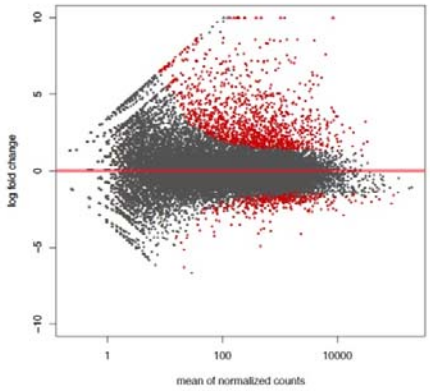

C

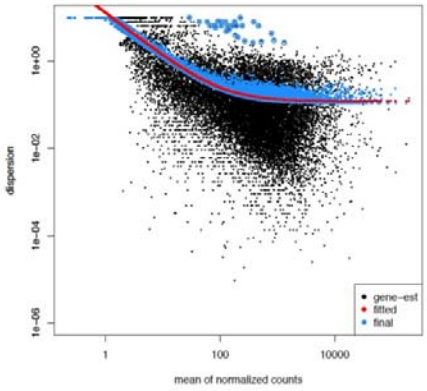

Figure S7

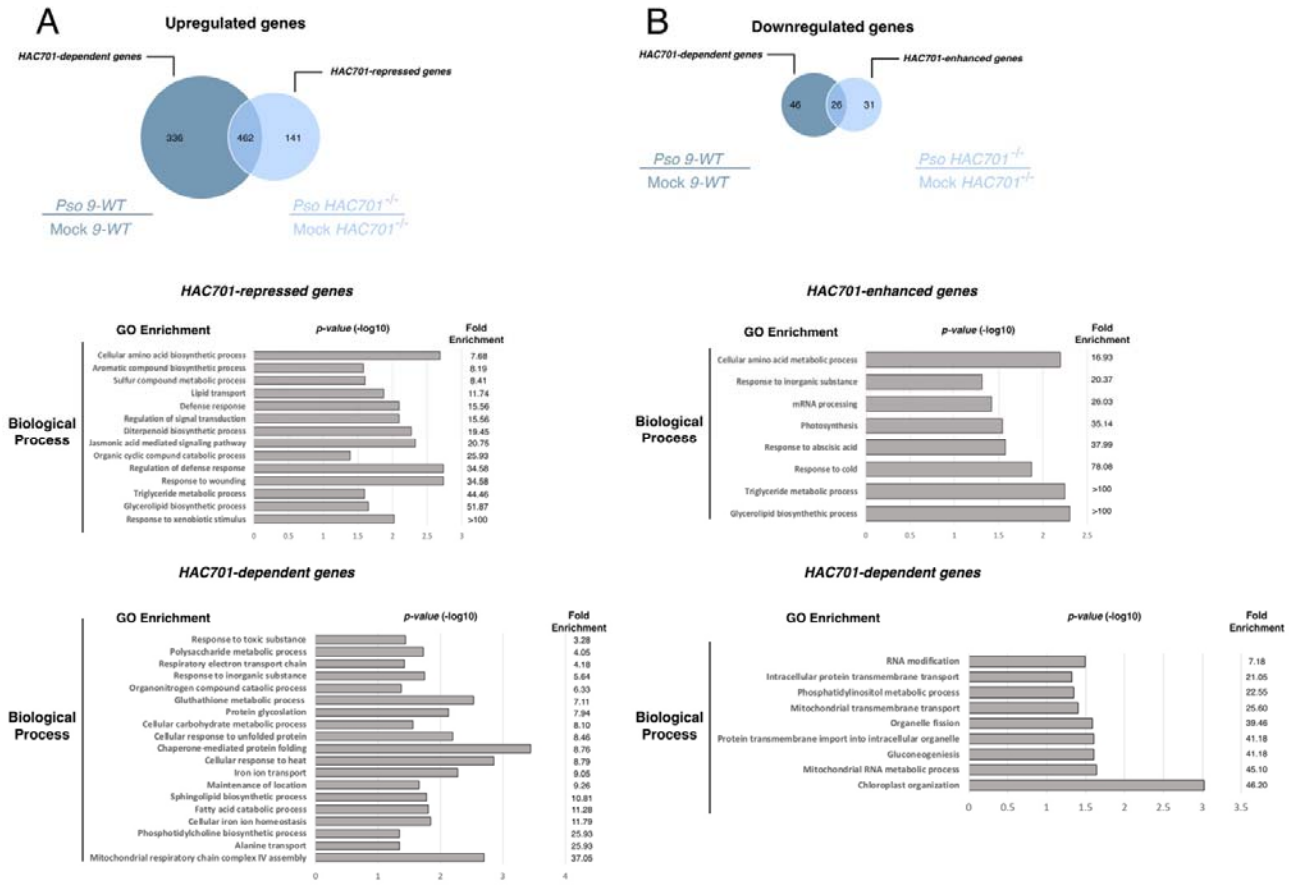
A
Upregulated genes
HAC701-dependent genes
HAC701-repressed genes
336
462
141
Pso 9-WT
Mock 9-WT
Pso HAC701-/-
Mock HAC701-/-
B
Downregulated genes
HAC701-dependent genes
HAC701-enhanced genes
46
26
31
Pso 9-WT
Mock 9-WT
Pso HAC701-/-
Mock HAC701-/-
HAC701-repressed genes
GO Enrichment
p-value (-log10)
Fold Enrichment
Biological Process
Cellular amino acid biosynthetic process 7.68
Aromatic compound biosynthetic process 8.19
Sulfur compound metabolic process 8.41
Lipid transport 11.74
Defense response 15.56
Regulation of signal transduction 15.56
Diterpenoid biosynthetic process 19.45
Jasmonic acid mediated signaling pathway 20.75
Organic cyclic compund catabolic process 25.93
Regulation of defense response 34.58
Response to wounding 34.58
Triglyceride metabolic process 44.46
Glycerolipid biosynthetic process 51.87
Response to xenobiotic stimulus >100
HAC701-enhanced genes
GO Enrichment
p-value (-log10)
Fold Enrichment
Biological Process
Cellular amino acid metabolic process 16.93
Response to inorganic substance 20.37
mRNA processing 26.03
Photosynthesis 35.14
Response to abscisic acid 37.99
Response to cold 78.08
Triglyceride metabolic process >100
Glycerolipid biosynthethic process >100
HAC701-dependent genes
GO Enrichment
p-value (-log10)
Fold Enrichment
Biological Process
Response to toxic substance 3.28
Polysaccharide metabolic process 4.05
Respiratory electron transport chain 4.18
Response to inorganic substance 5.64
Organonitrogen compound cataolic process 6.33
Gluthathione metabolic process 7.11
Protein glycosilation 7.94
Cellular carbohydrate metabolic process 8.10
Cellular response to unfolded protein 8.46
Chaperone-mediated protein folding 8.76
Cellular response to heat 8.79
Iron ion transport 9.05
Maintenance of location 9.26
Sphingolipid biosynthetic process 10.81
Fatty acid catabolic process 11.28
Cellular iron ion homeostasis 11.79
Phosphotidylcholine biosynthetic process 25.93
Alanine transport 25.93
Mitochondrial respiratory chain complex IV assembly 37.05
HAC701-dependent genes
GO Enrichment
p-value (-log10)
Fold Enrichment
Biological Process
RNA modification 7.18
Intracellular protein transmembrane transport 21.05
Phosphatidylinositol metabolic process 22.55
Mitochondrial transmembrane transport 25.60
Organelle fission 39.46
Protein transmembrane import into intracellular organelle 41.18
Gluconeogeniesis 41.18
Mitochondrial RNA metabolic process 45.10
Chloroplast organization 46.20

Figure S8

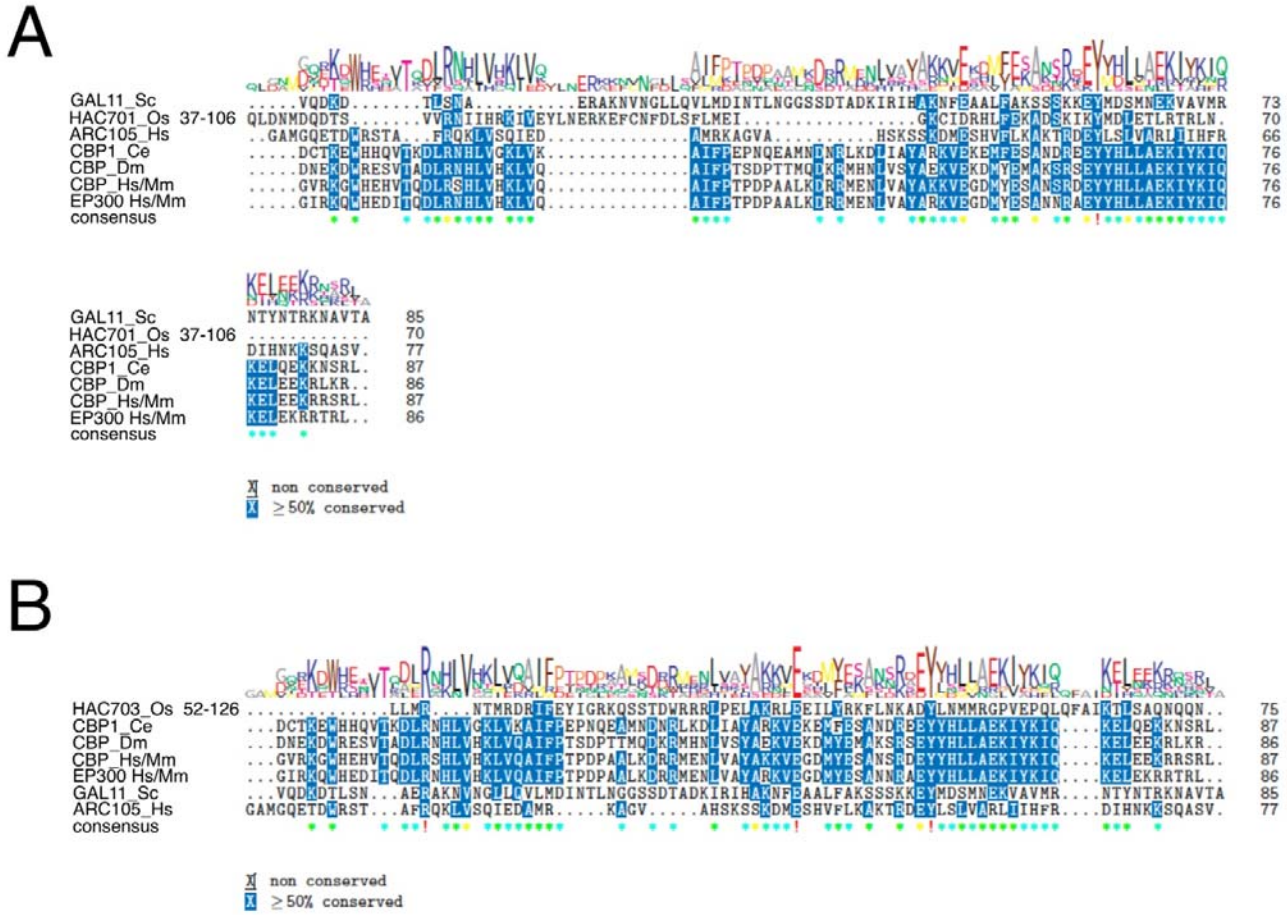
A
GAL11_Sc
HAC701_Os 37-106
ARC105_Hs
CBP1_Ce
CBP_Dm
CBP_Hs/Mm
EP300 Hs/Mm
consensus
NTYNTRKNAVTA
DIHNKKSQASV.
KEDQEKKNSRL.
KEDEEKRLKR..
KEDEEKRRSRL.
KEDEKRRTRL..
non conserved
≥50% conserved
B
HAC703_Os 52-126
CBP1_Ce
CBP_Dm
CBP_Hs/Mm
EP300 Hs/Mm
GAL11_Sc
ARC105_Hs
consensus
non conserved
≥50% conserved

Figure S9

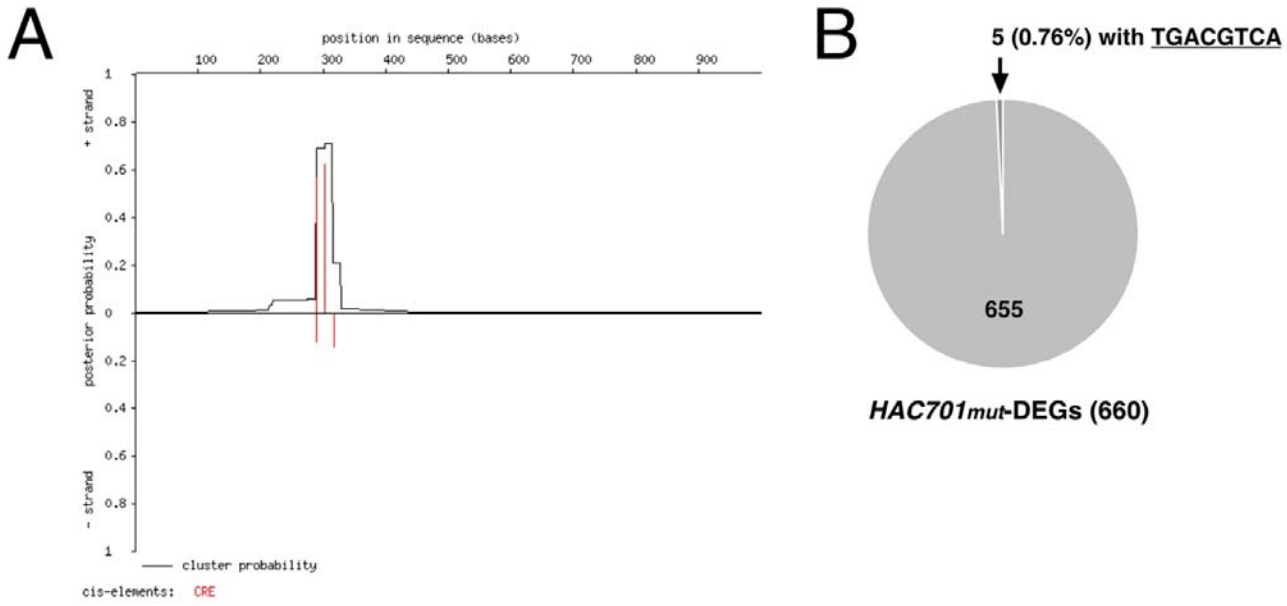

Possible functional cis-elements

Type	Position	Strand	Sequence	Probability
CRE	303-314	+	cgtgacgtcatc	0.62
CRE	289-300	+	gctgacgtcgcc	0.56
CRE	317-328	-	gttgtcgtcccc	0.14
CRE	289-300	-	gctgacgtcgcc	0.12

Figure S10

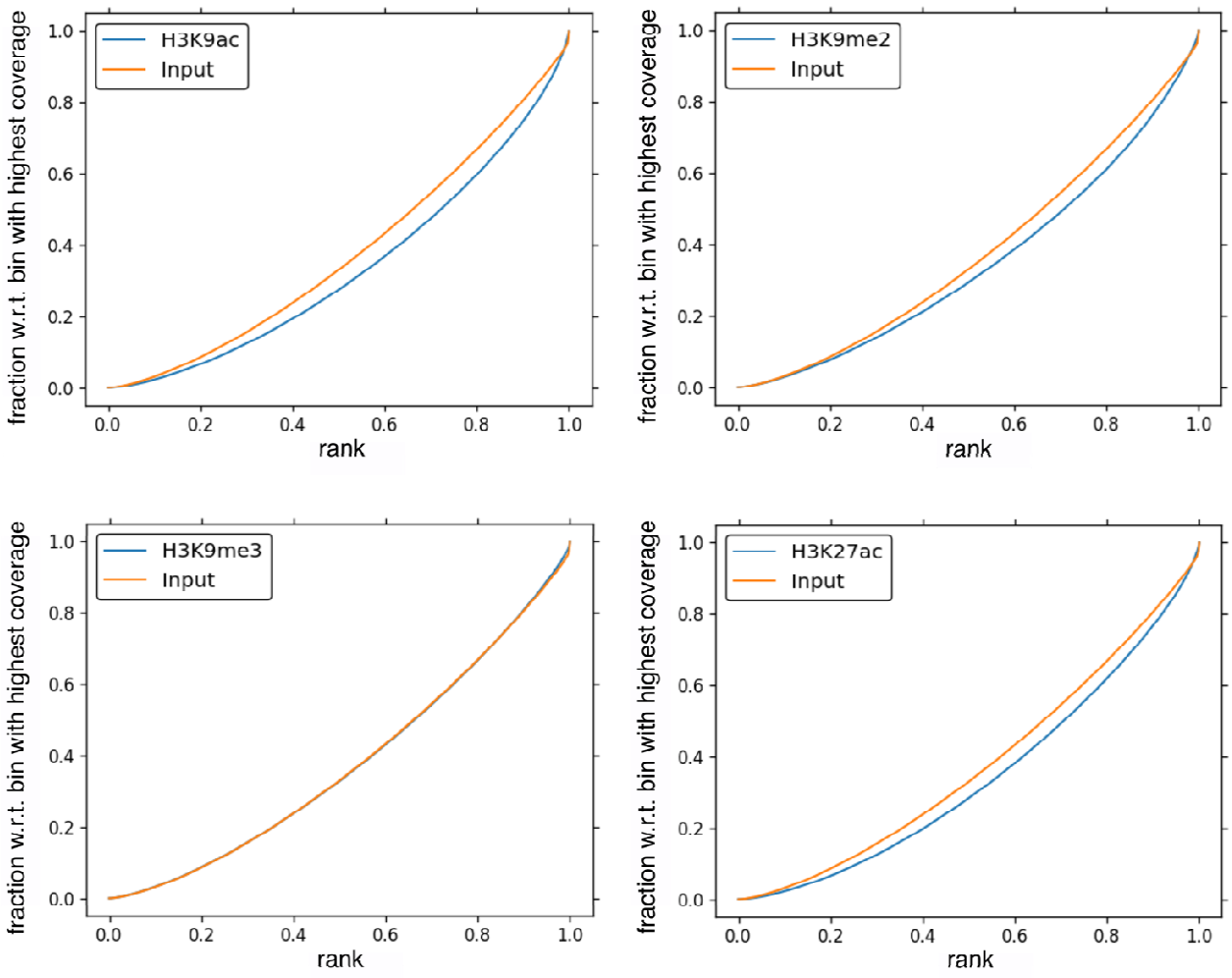
H3K9ac
Input
H3K9me2
Input
H3K9me3
Input
H3K27ac
Input
fraction w.r.t. bin with highest coverage
rank
0.0
0.2
0.4
0.6
0.8
1.0

Figure S11

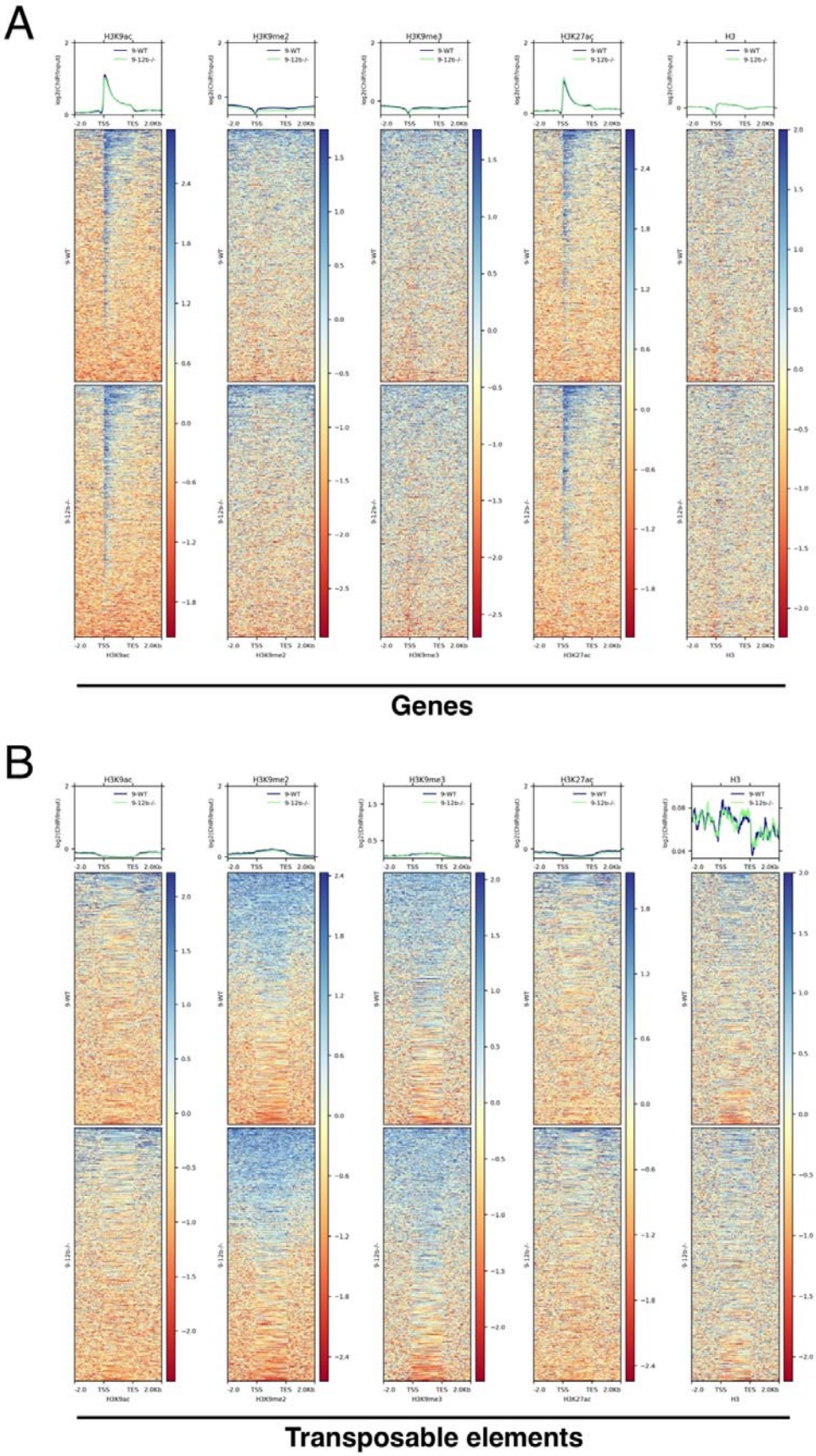
A
H3K9ac
H3K9me2
H3K9me3
H3K27ac
H3
9-WT
9-12b-/-
-2.0 TSS TES 2.0Kb
Genes
B
Transposable elements

Figure S12

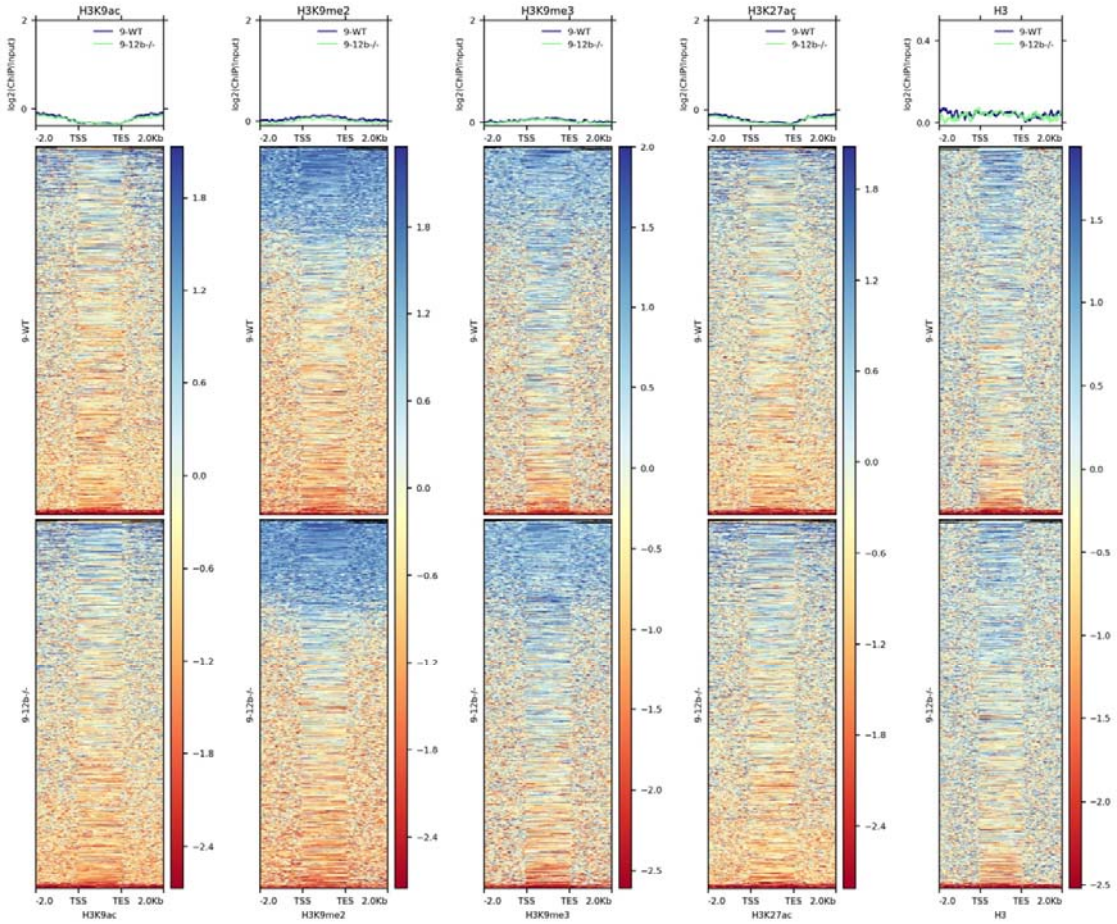

Simple Repeats

Figure S13

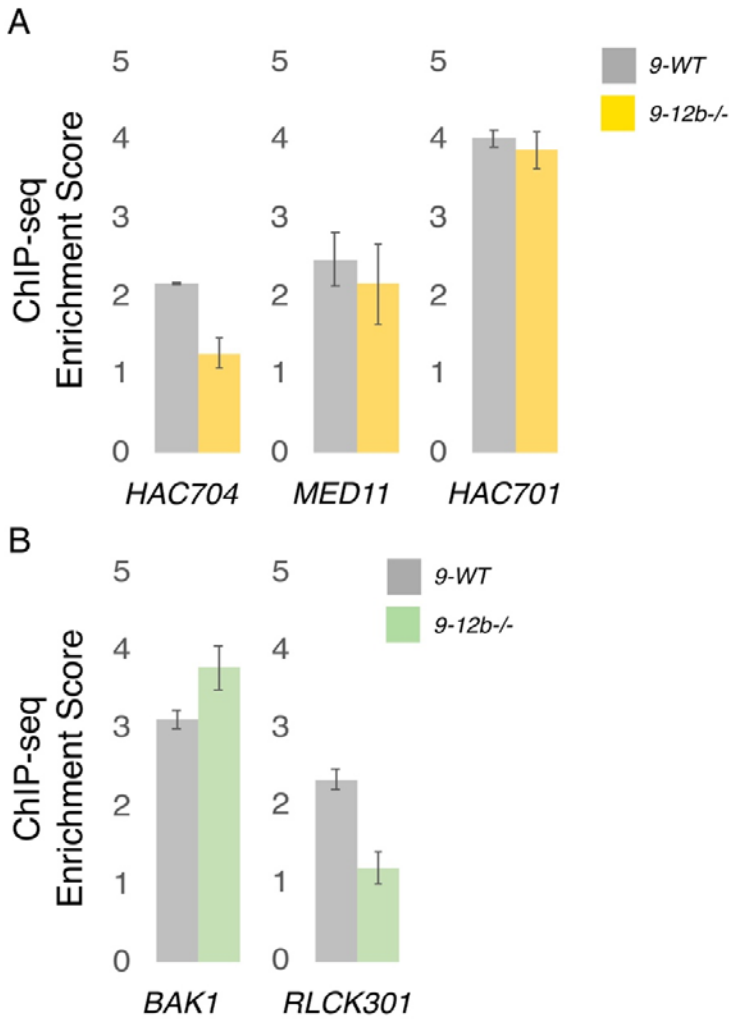
A
ChIP-seq
Enrichment Score
0
1
2
3
4
5
HAC704
MED11
HAC701
9-WT
9-12b-/-
B
ChIP-seq
Enrichment Score
BAK1
RLCK301
9-WT
9-12b-/-

Figure S14

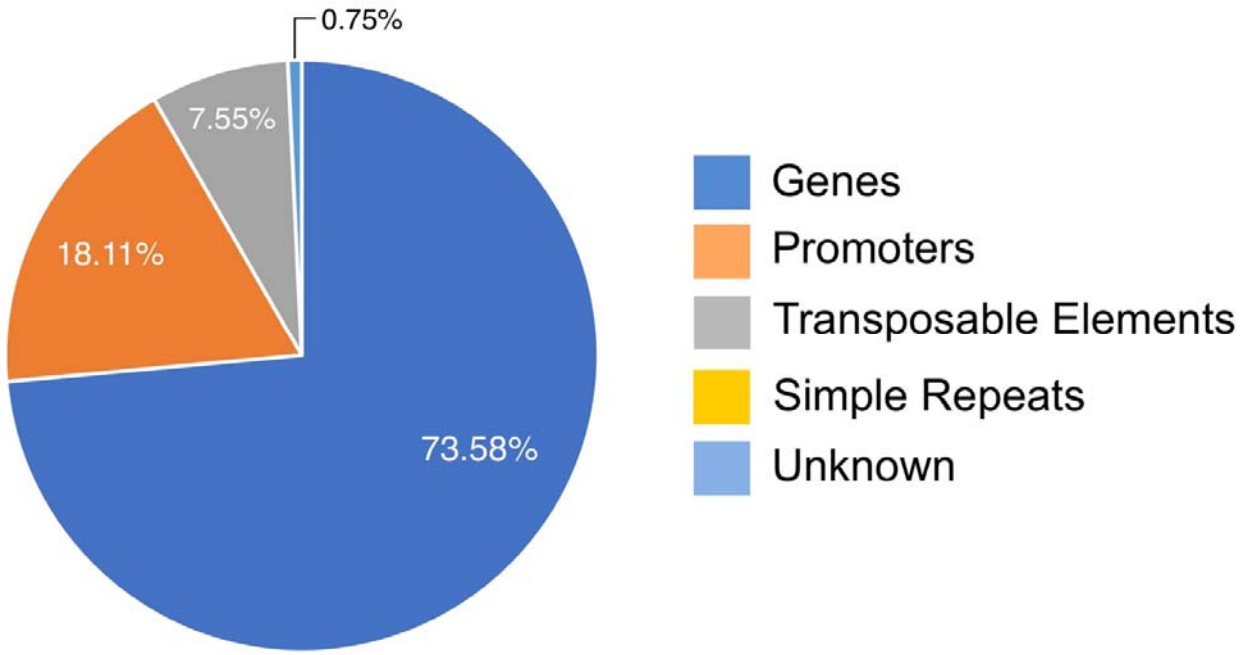
0.75%
7.55%
18.11%
73.58%
Genes
Promoters
Transposable Elements
Simple Repeats
Unknown

Figure S15

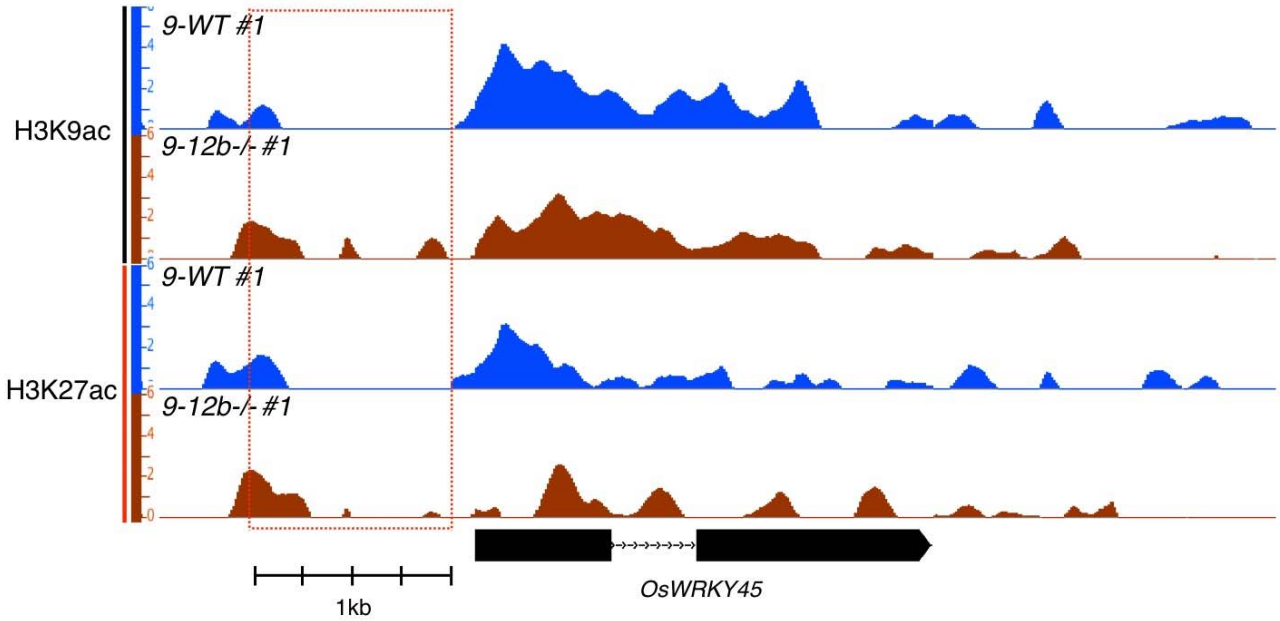

Figure S16

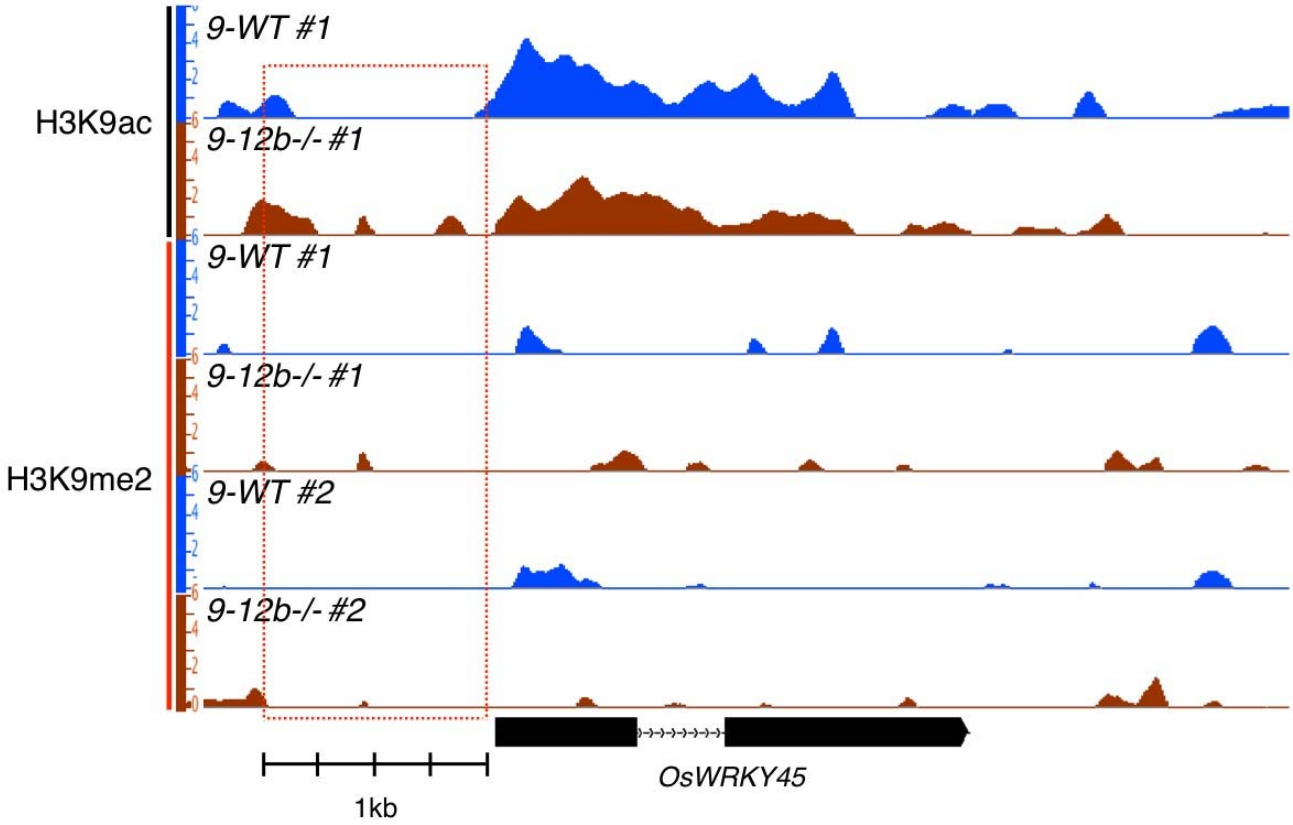
H3K9ac
9-WT #1
9-12b-/- #1
H3K9me2
9-WT #1
9-12b-/- #1
9-WT #2
9-12b-/- #2
OsWRKY45
1kb

Figure S17

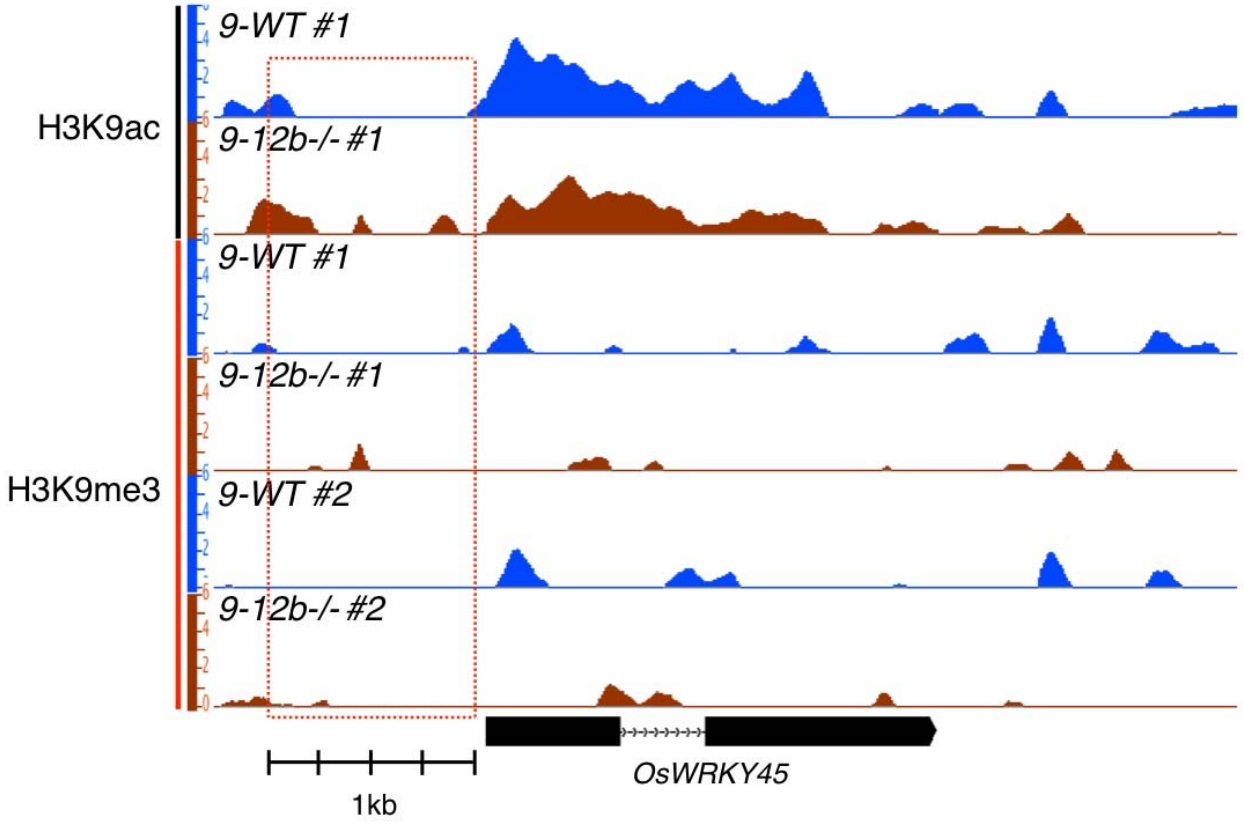
H3K9ac
9-WT #1
9-12b-/- #1
H3K9me3
9-WT #1
9-12b-/- #1
9-WT #2
9-12b-/- #2
OsWRKY45
1kb

Figure S18

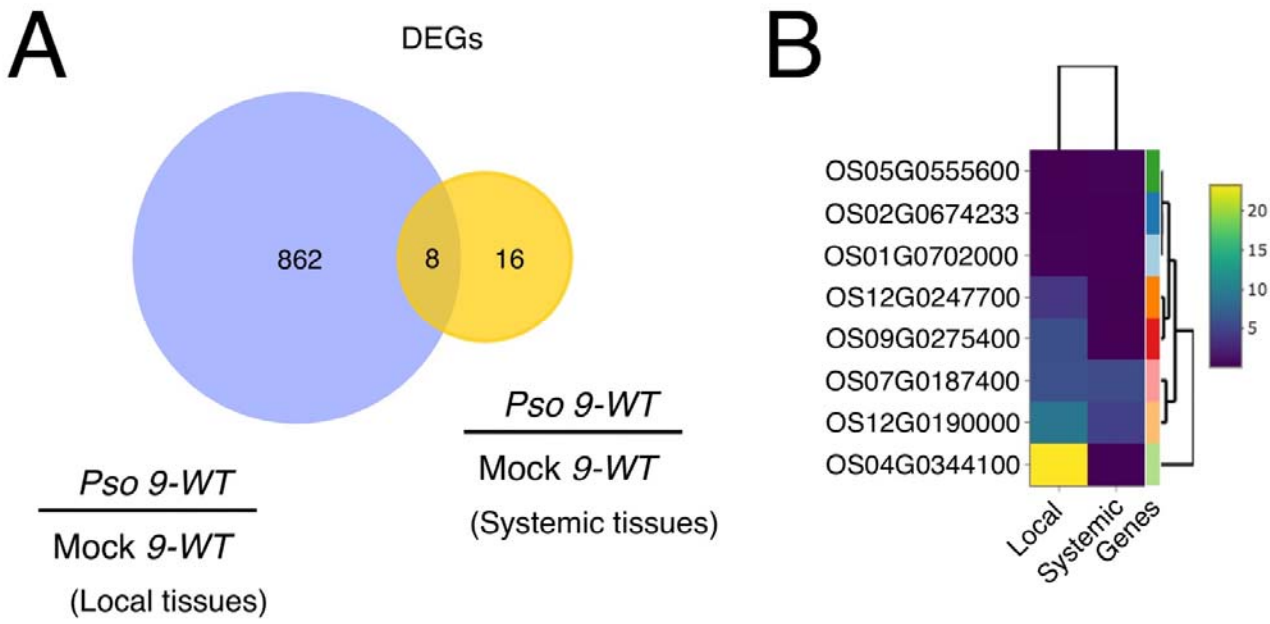
A
DEGs
862
8
16
Pso 9-WT
Mock 9-WT
(Local tissues)
Pso 9-WT
Mock 9-WT
(Systemic tissues)
B
OS05G0555600
OS02G0674233
OS01G0702000
OS12G0247700
OS09G0275400
OS07G0187400
OS12G0190000
OS04G0344100
Local
Systemic
Genes
20
15
10
5

Figure S19

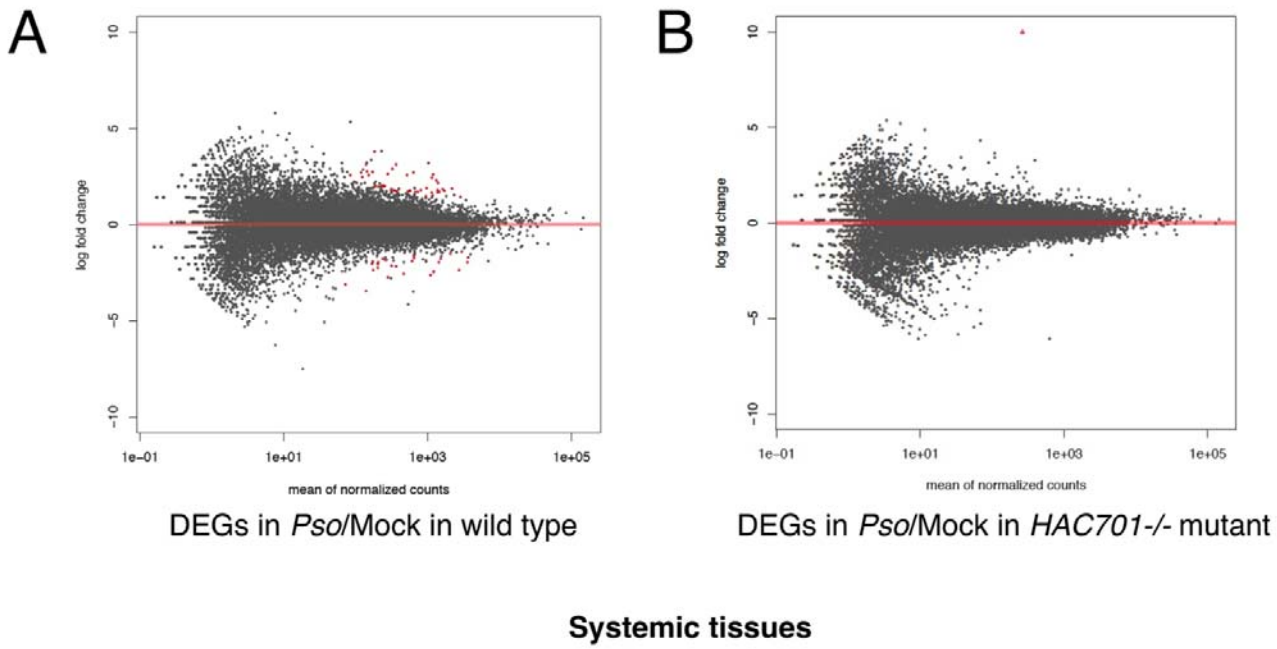

Systemic tissues

Figure S20

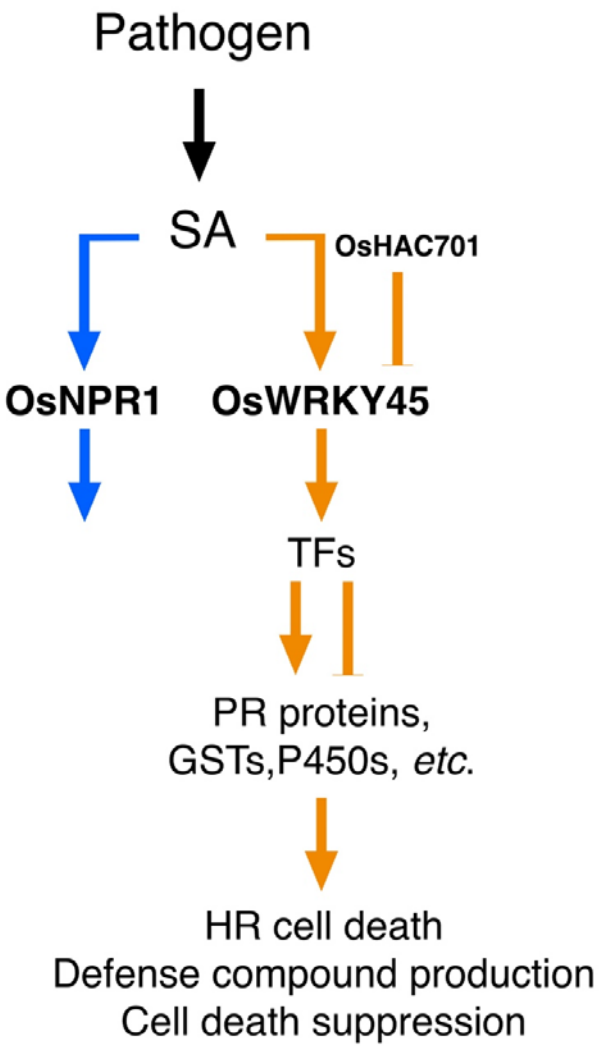
Pathogen
SA
OsHAC701
OsNPR1
OsWRKY45
TFs
PR proteins,
GSTs,P450s, etc.
HR cell death
Defense compound production
Cell death suppression